NJC

ROYAL SOCIETY OF CHEMISTRY

PERSPECTIVE

View Article Online
View Journal | View Issue

Cite this: *New J. Chem.*, 2022, **46**, 4514

Borophene as a rising star in materials chemistry: synthesis, properties and applications in analytical science and energy devices

Dharaben J. Joshi, Naved I. Malek and Suresh Kumar Kailasa *

Received 5th November 2021,
Accepted 27th January 2022

DOI: 10.1039/d1nj05271c

rsc.li/njc

Borophene is a two-dimensional (2D) material that has shown outstanding applications in energy storage devices. In recent years, borophene has been identified as a rising star in materials chemistry for the development of sensors, batteries and energy storage devices. This review provides an overview on synthetic strategies for the preparation of borophene nanostructure materials as well as their properties (mechanical, thermal conductivity, magnetic, structural, optical and electronic). Further, the applications of borophene nanostructure materials in sensing, battery recharge and hydrogen storage are discussed. Finally, we discuss the summary and future perspectives of borophene nanostructure materials in multidisciplinary research.

1. Introduction

Graphene[1,2] and other two-dimensional (2D) nanomaterials, such as hexagonal boron nitride,[3,4] silicene,[5–9] germanene[10] and phosphorene,[11] have received increasing interest over the past decade (Fig. 1). The use of 2D materials, as well as certain previously undiscovered 2D materials, has been proposed theoretically.[12] 2D materials offer unique physicochemical properties, such as electrical and thermal conductivity, band structure around the Fermi level, and toughness. Thus, borophene is widely used as a potential material for various applications.[13] The current study offers the primary experimental design to demonstrate the feasibility of new boron nanostructures with hexagonal positions. Due to the lack of electrons, boron could

Department of Chemistry, Sardar Vallabhbhai National Institute of Technology, Surat – 395007, Gujarat, India. E-mail: sureshkumarchem@gmail.com, skk@chem.svnit.ac.in

Dharaben J. Joshi

Dharaben J. Joshi was born in 1996 in Amreli, Gujarat, India. She obtained her BSc degree from Saurashtra University (Kamani Science College And Prataprai Arts College, Amreli) in 2017 and MSc degree from the Department of Chemistry, Sardar Patel University, in 2019. She qualified for the CSIR National Eligibility Test in 2018. Currently, she is pursuing her doctoral research under the guidance of Dr K. Suresh Kumar in the Department of Chemistry, SVNIT, Surat, Gujarat.

Naved I. Malek

Naved Malek is working as an Associate Professor at Sardar Vallabhbhai National Institute of Technology (SVNIT), Institute with National Importance. He is also a Fellow of the Royal Society of Chemistry, UK. He has established the Ionic Liquid Research Laboratory at the Department of Chemistry, SVNIT. He has worked as a Postdoctoral Fellow at the University of Sao Paulo, Sao Paulo, Brazil, with Prof. Omar El Seoud. Dr Malek has more than 17 years of research experience. He has completed several research projects under various funding agencies from India and abroad. He is a co-author of 5 book chapters and 91 research papers in journals of international repute, and has more than 1400 citations with an h-index of 23 and i10-index of 52.

not make a graphene-like structure but the computational study proposed that partially filled hexagonal extended boron sheets are stable, which allows them to exhibit borophene nanostructures just like graphene. However, there is no experimental indication for such atom-thin boron nanostructures. Borophene is a one-atom-thick boron sheet constructed by the planar hexagonal B_{36} unit.[14] The newly discovered borophene involves a single layer of boron atoms synthesized in ultra-high vacuum on a silver (Ag) substrate.[15,16] Four phases of borophene (2-*Pmmn*, β12, χ3, and honeycomb) have been produced with a metallic nature. Many experimental and theoretical investigations of borophene have revealed its mechanical characteristics, electrical structure, optical properties, atomic adsorption, and surface reactivity.[16,17] Borophene with the 2-*Pmmn* phase is an example of a buckled structure, with neighbouring row boron atoms corrugated in a zigzag pattern. The atomic structure is uncorrugated in the opposite in-plane direction. Surprisingly, the Poisson's ratios are negative for both in-plane directions.[18]

Pnictogens and other mono-elemental layered materials have been the subject of many first-principles investigations to better understand them and explore their efficient

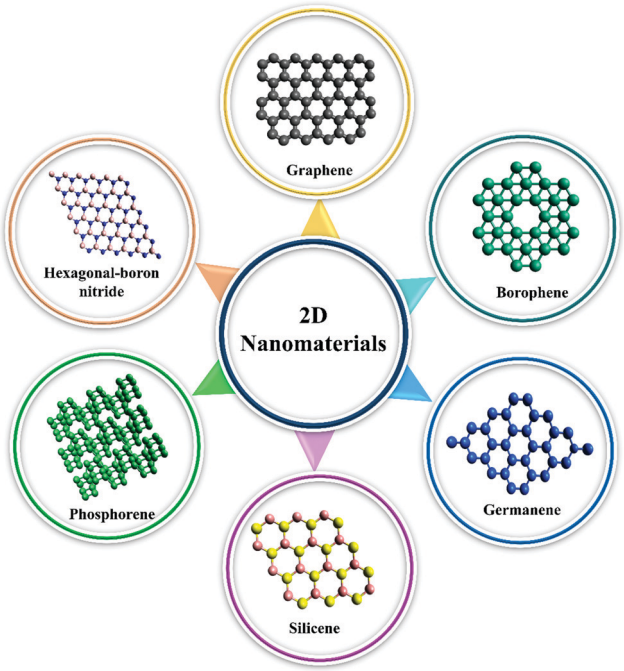

Fig. 1 Structures of different types of 2D nanomaterials.

Suresh Kumar Kailasa

Suresh Kumar Kailasa, FRSC, is an Associate Professor of the Department of Chemistry at Sardar Vallabhbhai National Institute of Technology (SVNIT) Surat, Gujarat, India. He obtained his Master of Science degree in the Chemistry of Natural Products from Sri Krishnadeveraya University, Andhra Pradesh, India, and PhD in Chemistry from Sri Venkateswara University, Tirupati, Andhra Pradesh, India. After completing two postdoctoral fellowships at Chonbuk University, South Korea, and at National Sun Yat-Sen University, Taiwan, he joined as an Assistant Professor at SVNIT, Surat, in 2009. He received the Young Scientist Award from the Taiwan Mass Spectrometry Society in 2013. He was selected as a Brain Pool Scientist at the Department of Chemistry, Chung-Ang University, South Korea, under the Korean Brain Pool Invitation Program of KOFST in 2017. He acted as a Guest Editor for special issues of Applied Sciences (MDPI) and Materials Today Chemistry (Elsevier). Currently, he is the head of the Department of Chemistry, SVNIT, Surat, India. He is the author of 172 peer-reviewed papers and is the co-inventor of a Taiwan Patent. He has an h-index of 43 and has accumulated over 6113 citations. Recently, he has been featured in the top 2% of scientists compiled by Stanford University in the USA. His research interest is in the field of analytical chemistry, MALDI-MS, ESI-MS, microextraction, nanosensors, drug delivery, surface modifications of nanostructure materials, and functional nanomaterials for the development of new analytical strategies.

performance. Despite this, the translation of theoretical studies into actual prospective applications has not been fully realized or thoroughly researched.[19] The electrical band structure is extremely anisotropic because of the anisotropic crystal structure. It was noticed that the band structure exhibited a metallic nature in the armchair direction. However, there is a significant bandgap in the zigzag direction.[20] Noticeably, borophene was exploited as a gas sensor *via* computational approaches.[21] The gas-sensing mechanism and adsorption phenomenon of gas molecules on borophene surfaces are currently unknown. However, researchers are trying to better understand the above mechanisms using microscopic and computational studies.[21] It has been discovered that ultra-fast surface ion transport may occur in the armchair direction. Furthermore, borophene exhibited high capacity and good electronic conductivity, and may be a promising material in batteries because of its large capacity, and excellent electronic and ionic conductivity.[22] The metal-functionalized borophene exhibited high ability to adsorb more number of H_2 molecules.[23] It was confirmed that metal-decorated borophene exhibited remarkable H_2 storage capacity due to the lower mass of the boron and metal.[23]

In this review, we discuss the brief history of borophene as a 2D material and also discussed the different computational methods used for the characterization and calculations of borophene nanomaterials. We discuss the properties (optical, magnetic, electrical, thermal conductivity, mechanical and physicochemical) of the borophene nanostructure materials. Then, we highlight the potential applications of borophene nanomaterials in batteries ((sodium ion batteries (NIBs)), (lithium-ion batteries, (LIBs)), and other batteries), gas sensing and H_2 storage devices. Finally, we discuss the future perspective of borophene-based nanomaterials in various fields of science and technology.

1.1. History of borophene

Guisinger *et al.* succeeded in synthesizing single-layer borophene with ultra-thin nanostructures on a pure Ag substrate at high temperatures in ultrahigh vacuum settings utilizing boron vapor as the boron source in 2015.[24] Owing to the complicated bonding processes with bulk boron's non-layered structure, the experimental synthesis of borophene was not accomplished until a team of research groups independently synthesized borophene on Ag(111) in 2015.[24,25] At the same time, scientists planned a new notation, BC (n, m), in which n = narrowest areas and m = largest regions, specifying the number of the widest regions.[26] Researchers demonstrated that ultra-sonication-assisted liquid-phase exfoliation may produce multilayer borophene with high quality, and regulated size and thickness.[27] Similarly, borophene was efficiently grown on the surfaces of Ag(111) and Cu(111). The borophene crystal structure and properties have been investigated using density functional theory (DFT), scanning tunneling microscopy (STM), and low-energy electron microscopy.[28]

2. Computational methods

DFT was utilized to make the computational design of borophene, which includes the structural optimization and calculations of borophene with key features. The Amsterdam density functional (ADF) package with BAND and DFTB modules was used in the linear combination of atomic orbital (LCAO) method.[28] Noticeably, the exchange correlation interaction of the electrons was estimated by using the Perdew–Burke–Ernzerhof scheme (PBE) with generalized gradient approximation (GGA) models.[29] The correct behaviour around the nucleus was investigated by the Slater-type orbital (STO) basis functions.[30] The electronic and atomic wavefunctions were represented using an exact basis set of triple zeta double polarization.[31] During the SCF cycles, the structures were completely stable to produce geometrically optimized structures, and integration of the numerical data was carried out using the tight convergence criteria of 1×10^{-6} eV.[32,33] It was noticed that borophane exhibited dynamic stability, whereas borophene is structurally unstable, illustrating that a stable borophene could be produced by using a suitable substrate.

3. Synthetic strategies for the preparation of borophene

Borophene is unstable and requires an effective substrate to stabilize. Xu's group theoretically predicted a fully hydrogenated borophene.[34] Hydrogenated borophene is collectively referred to as borophane. This section is completely dedicated to the fabrication of borophene using various synthetic strategies.

3.1. Growth of borophene on the metal surface

To explore the borophene applications, a single layer borophene was produced *via* the self-assembly of boron on the surface of Ag(110).[25] The Mannix group prepared a 2D boron nanostructure *via* self-assembly of boron onto the surface of Ag under ultrahigh-vacuum conditions.[24] The relative concentration on the surface of Ag was highly dependent on the growth temperature and deposition rate. The formation of the striped phase was due to the low deposition rate and increase in growth temperature. Feng *et al.* produced a 2D boron nanosheet on the Ag(111) substrate.[19] In this strategy, β12 and χ3 boron sheets were generated and exhibited a triangular lattice. The formed boron sheets showed different arrangements of periodic holes, which were confirmed by STM. First-principles calculations and *ab initio* molecular dynamics simulations were conducted for the electronic properties and atomic structure of the 2D boron sheet (borophene) on the Ag(111) surface.[35] These studies demonstrated that the 2D boron sheet exhibit three borophene nanostructures (β5, χ1, and χ2) with good stability. The formed borophene is in a planar structure with slight surface buckling (~0.15 Å). Another synthetic strategy was also demonstrated for the preparation of 2D borophene on the Ag(111) substrate.[36] The Campbell group demonstrated the use of Ag(111) as a promising substrate for the production of atomically thin boron sheets (borophene).[37] The formed borophene exhibited a vdW-like structure, revealing that the formed borophene does not contain a bulk allotrope structure. The formation of borophene was closely investigated by STM and low-energy electron microscopy, and modeled by *ab initio* theory.[27] Authors noticed that the growth of borophene on the Cu(111) substrate offers the formation of large single-crystal domains with the size of 100 μm^2, exhibiting novel triangular nanoarchitectures with hexagonal vacancies (η = 1/5).

Another synthetic method was the efficiently produced borophene nanostructures onto the Al(111) substrate under ultrahigh vacuum.[38] The STM data revealed that the formed borophene is a monolayer that exhibits a planar, non-buckled honeycomb lattice, which is very similar to the graphene structure. The Zhu group investigated the energetic, structural, lattice dynamic and electronic properties of the honeycomb borophene that was produced onto the Al(111) substrate through *ab initio* calculations.[39] Furthermore, different layers of the 2D boron sheets were efficiently grown onto a SiN_x surface using a plasma-assisted ion implantation tool.[40] Kiraly *et al.* explored the use of the Au(111) substrate for the growth of borophene with a trigonal network.[41] Authors noticed that the borophene islands were formed across the Au(111) surface using low amounts of boron. Recently, the growth of the nanostructure borophene onto the Ag(111) surface was investigated by DFT calculations.[42]

3.2. Liquid-phase exfoliation method

Exfoliation is one of the simple routes for the fabrication of a wide variety of nanostructure materials. Recently, the exfoliation strategy has been proven to be a promising synthetic route for the preparation of borophene. For example, large quantities of borophenes were synthesized using $NaBH_4$ as a reagent and H_2 as a carrier gas *via in situ* thermal decomposition.[43] In this approach, borophene was grown without the use of a metal substrate, showing good crystalline structures with good stability when they dispersed in a base or strong acid as a solvent. Similarly, large-scale atomic sheets of borophene were synthesized

via the liquid-phase exfoliation approach.[44] Authors noticed the formation of a mixture of borophene (β12, X3, and their intermediate phases) and reduced borophene oxide, which were confirmed by STM and X-ray photoelectron spectroscopic techniques (XPS). Noticeably, the formed borophene oxide exhibited a specific capacity at ≈4941 mA h g^{-1}, which is remarkably higher than that of other 2D nanomaterials and their hybrids. Similarly, large scale high quality few-layer borophene nanosheets were obtained *via* ultrasonication, followed by liquid-phase exfoliation.[26] The few atomic-layer borophene nanosheets were produced from bulk boron powder (2 μm) *via* the ultra-sonication-mediated liquid-phase exfoliation approach using dimethylformamide (DMF) and isopropyl alcohol (IPA) (1 mg mL^{-1}) as a solvent (Fig. 2). Scanning electron microscopic (SEM) images demonstrated that the as-synthesized borophene *via* DMF-exfoliation showed high transparency with dimensions from a few nm to μm, as compared to the bulk boron powder (Fig. 2b–d). Importantly, the formed borophene exhibited remarkable stability in organic solvents without any agglomeration and was stable for more than 50 days at room temperature. The authors used UV-Visible spectroscopy for the estimation of the dispersion ability and optical characteristics of borophene (Fig. 3). The color of the IPA- and DME-exfoliated borophene sheets was changed from a dark brown to a light yellow color with respect to the concentration of borophene from higher to lower concentration (Fig. 3a and d). Furthermore, the dispersion ability of the prepared few atomic layer borophene nanosheets was investigated by measuring the absorbance of the borophene sheets in both solutions at λ = 504 and 400 nm for IPA and DMF, demonstrating that the borophene nanosheets are well dispersed in the DMF and IPA solvents (Fig. 3b and e). The colloidal nature of the prepared borophene was confirmed by studying the Tyndall effect in both solvents, illustrating that the prepared borophene is in colloidal nature. Moreover, the obtained borophene in DMF showed higher stability than borophene in IPA (Fig. 3c and f).[26]

Recently, a new type of borophene quantum dots (QDs) was synthesized *via* the ultrasonication-mediated liquid-phase exfoliation approach at low temperature.[45] In this strategy, hydrogen peroxide, boric acid and IPA were used for the fabrication of borophene QDs, where boric acid is an essential reagent for the preparation of borophene QDs. Furthermore, ultra-small borophene QDs were produced with a narrow size distribution using hydrogen peroxide, confirming that hydrogen peroxide acts as reagent to create a higher liquid–gas interface to peel the boron particles. A novel synthetic strategy was developed for the preparation of few-layers borophene with large flake sizes *via* the solvothermal-mediated liquid phase exfoliation approach.[46] Authors studied the effect of various solvents, including *N*,*N*-dimethyl formamide (DMF), acetone, ethanol, acetonitrile, and *N*-methyl pyrrolidone (NMP), for the exfoliation of borophene. Among these, acetone was found to be the best solvent for the synthesis of borophene with four-layer thickness and a mean size of 5.05 μm. These liquid-phase exfoliation strategies demonstrated that the few-layers borophene nanostructure was effectively fabricated with outstanding properties. Furthermore, the advances in the synthetic protocols opens new pathways to generate atomic layer borophene with precise size distribution, which will accelerate them as a promising material for various applications.[47] The 2D boron monolayers were successfully produced *via* chemical vapor deposition (CVD) method, and thin 2D γ-boron films were grown on copper foils by using boron oxide and pure boron powders as the boron source and H_2 gas as the carrier gas.[48] Furthermore, uniform crystalline semiconductor boron quantum dots (BQDs) were prepared in large scale by using bulk boron powders in acetonitrile *via* ultrasonication method.[49] The as-synthesized BQDs were further characterized by photoluminescence and UV-Visible spectroscopic techniques, confirming the strong quantum confinement effect.[49] Using the surface structure-search method and cluster expansion method, Zhang *et al.* synthesized metal substrate-dependent 2D boron.[50] For the

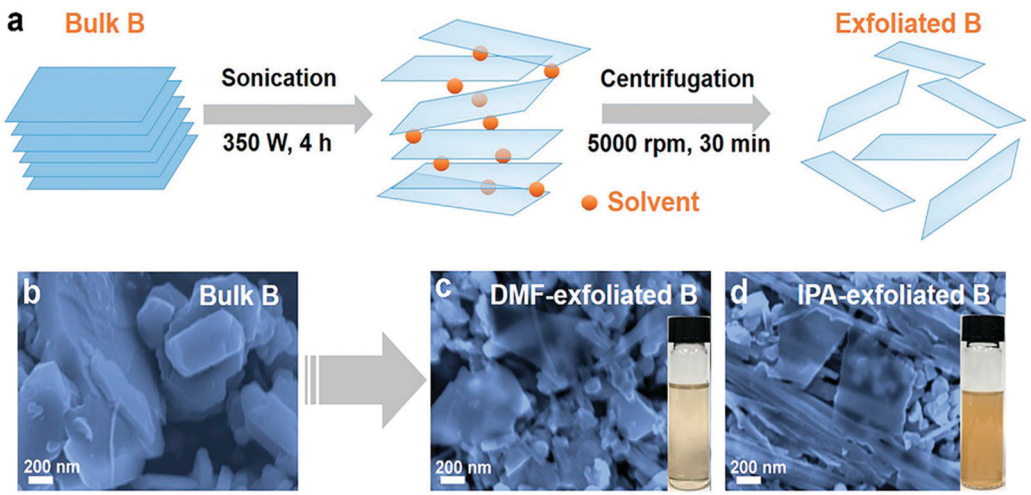

Fig. 2 (a) Schematic representation of the synthesis of borophene *via* sonication-assisted liquid-phase exfoliation. SEM images of (b) bulk borophene and borophene nanosheets produced by tip-sonication in (c) DMF and (d) IPA (d). Insets: (c) and (d) Show borophene dispersed in DMF and IPA, respectively. This figure has been reproduced from ref. 26 with permission from American Chemical Society, copyright 2018.

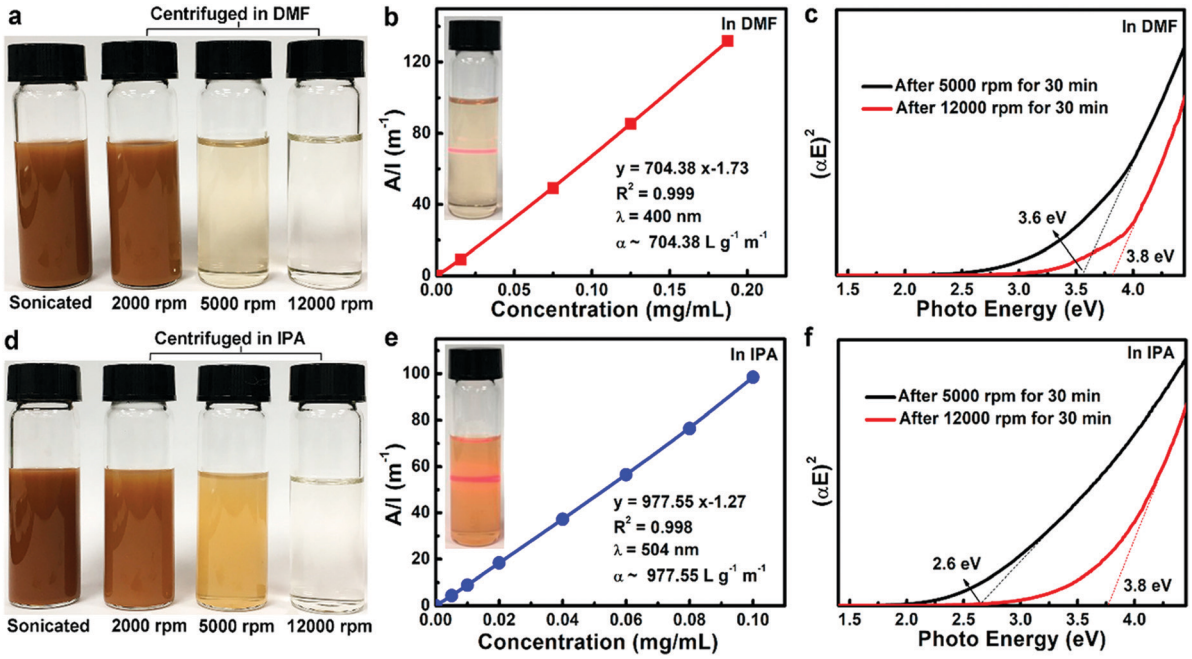

Fig. 3 Photographic images of borophene nanosheets dispersed in (a) DMF and (d) IPA. Absorbance (A, at λ = 400 nm for DMF and λ = 504 nm for IPA) of borophene measured as a function of DMF-exfoliated (b) and IPA-exfoliated (e) borophene nanosheet dispersion. Tauc plots were constructed for the optical absorption data of the DMF-exfoliated (c) and IPA-exfoliated (f) few-layer borophene nanosheet dispersions at different centrifugation speeds of 5000 and 12 000 rpm for 30 min. This figure has been reproduced from ref. 26 with permission from American Chemical Society, copyright 2018.

as-synthesized 2D boron on highly reactive Cu, Ni and Ag, the most stable specific planer structure was found and raised in polymorphic energy degeneracy. Meanwhile, on the less interacting Au, there was significant buckling with nonplanar and numerous polymorphs as in vacuum.[50]

4. Properties of borophene

High Young's modulus, thermal and electric conductivities, and a changeable band gap are unique characteristics of borophene. The interlayer spacing, mechanical properties, and crystal structure are all essential because they affect the electrical and ionic conductivity, interlayer spacing, and structural stability of borophene.[51] This section describes the key properties of borophene.

4.1. Mechanical properties

When a material is subjected to an external force, it develops mechanical properties. To characterize the performance, constants of elastic stiffness may be employed. The four nonzero elastic stiffness constants are used in the stress–strain formula for the orthogonal symmetry under plane stress:[52]

$$\begin{pmatrix} \sigma_{xx} \\ \sigma_{yy} \\ \sigma_{xy} \end{pmatrix} = \begin{pmatrix} C_{11} & C_{12} & 0 \\ C_{21} & C_{22} & 0 \\ 0 & 0 & C_{44} \end{pmatrix} \begin{pmatrix} \varepsilon_{xx} \\ \varepsilon_{yy} \\ \varepsilon_{xy} \end{pmatrix} \quad (1)$$

where the tension and strain components are σ_{ii} and ε_{ii} respectively. These elastic stiffness constants C_{11}, C_{12}, C_{22} and C_{44} are in GPa, correspondingly, and used to calculate the constants.

$$E_x = \frac{C_{11}C_{22} - C_{12}^2}{C_{22}} \quad E_y = \frac{C_{11}C_{22} - C_{12}^2}{C_{11}} \quad \nu_{xy} = \frac{C_{11}}{C_{22}} \quad \nu_{xy} = \frac{C_{12}}{C_{21}} \quad (2)$$

Similarly, the constants for all angles were computed for the Young's modulus (Y_a, Y_b) and Poisson's ratio (ϑ_a, ϑ_b). Young's modulus and Poisson's ratio for all angles may be calculated using the following formula for the borophene model, which has orthogonal symmetry:[53]

$$Y(\theta) = \frac{C_{11}C_{22} - C_{12}^2}{C_{22}\cos^4\theta + A\cos^2\theta\sin^2\theta + C_{11}\sin^4\theta}.$$

where the $A = \frac{(C_{11}C_{22} - C_{12}^2)}{C_{66} - 2C_{12}}$, $B = \frac{C_{11} + {}_{22} - (C_{11}C_{22} - C_{12}^2)}{C_{66}}$.

A team of scientists discovered that the Young's modulus of fully hydrogenated borophenes (δ3, δ5 and stripped borophanes) is considerably lower than that of striped borophane (167.4 N m^{-1}), indicating that δ3 and δ5 borophanes have excellent flexibility. The estimated Poisson's ratios for δ3 and δ5 borophanes are higher than that for the striped borophane.[54] It was noticed that 248.26 and 321.54 N m^{-1} values were obtained for 8-*Pmmn* borophene Y_a and Y_b, respectively. Y_b decreased significantly as the hydrogen coverage increased. $BH_{1/2}$ had a Y_b of 218.38 N m^{-1}. Fig. 4 illustrates the polar diagrams of the Young's modulus and shear modulus in 2D borophene nanosheets.[55] The mechanical characteristics of the single layer 8-*Pmmn* borophene, such as the ideal strength and critical strain,

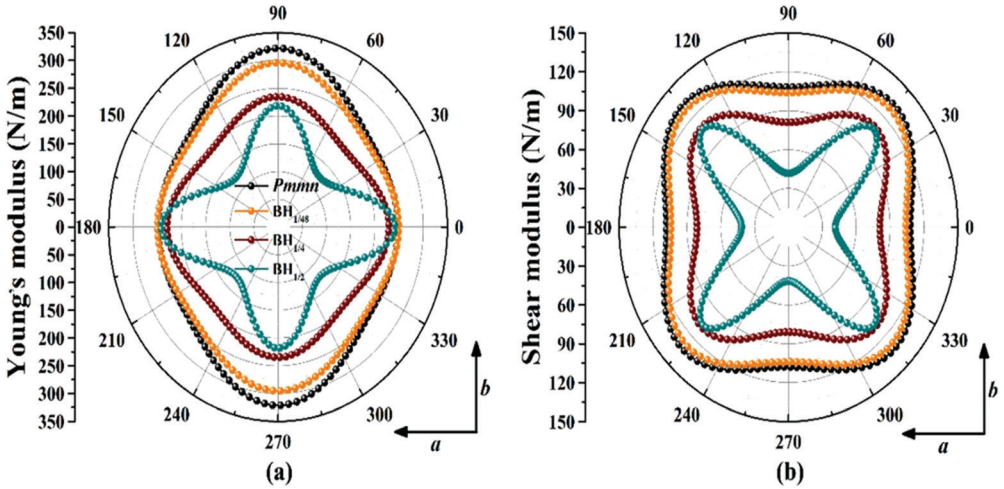

Fig. 4 Polar diagrams: (a) Young's modulus and (b) shear modulus in borophene phases (8-*Pmmn* borophene, $BH_{1/48}$, $BH_{1/4}$, and $BH_{1/2}$), in which the angle is calculated with respect to the *a*-axis. This figure has been reproduced from ref. 55 with permission from American Chemical Society, copyright 2019.

were studied, exhibiting good values. Authors noticed that the ultimate tensile strain is approximately 0.155 in the "*a*" direction and 0.16 in the "*b*" direction, which is higher than the striped borophene.[56] The elastic contact of h-B_2O and h-B_2H_2 is estimated to be 11.45 and 13.83 N m^{-1}, respectively, indicating that this material is mechanically stable.[57] In the armchair and zigzag directions, the Young's modulus is 236 and 89 GPa, respectively, demonstrating that borophene exhibits enormous mechanical anisotropy.[58] Despite the differing planes of atomic bonding and atomic mass density, β12 and χ3 borophene have comparable mechanical characteristics. One aspect of the striped borophene is the high rigidity and instability nature due to its strong directional bonding.[59] By increasing the number of layers, the critical stresses are increased, resulting in the generation of a more flexible structure than that of a monolayer structure. It was also noticed that when the layer number increased, the out-of-plane negative Poisson's ratios were maintained due to the buckling atomic structures.[60] The mechanical characteristics of the system are substantially altered by fluorination, showing notable findings, such as a direction-dependent change of the Young's modulus and a significant change in the transition from negative to positive Poisson's ratio of borophene and coverage levels of (BH_4 and BH_2) borophene.[61] Table 1 illustrates the mechanical characteristics of borophene.

4.2. Structural properties

The rectangular unit cell in the plane is visible in the top view of the borophene, which shows the two lattice bases values, *i.e.*, 2.866 and 1.614 Å, and the reciprocal lattices two basic vectors, 2.192 and 3.893 $Å^{-1}$. The unit cell contains two inequivalent boron atoms.[62] Along its armchair direction, B–B bonds were noticed in the parallel linear chains of the borophene nanostructures, leading to the generation of a remarkable buckling along its zigzag direction, which illustrated that the 2D borophene nanostructure has a highly anisotropic nature.[63] The X-ray technique was used to study the striped borophene stacked on top of graphene (sB-Gr). Furthermore, in sBGr, graphene is a buckled monolayer with a buckling height of 0.23 Å. Graphene, on the other hand, is not buckled in van der Waals (vdW) heterostructures.[64] For ease and efficiency, borophene was used instead of α′-boron sheet. In borophene, the planes are slightly buckled due the existence of coordination 6 in every two adjacent boron atoms. Borophene has an equivalent lattice constant of 4.37 Å and vertical distance from the plane of about 0.173 Å.[65] The experimental result confirms the α-sheet borophene adsorption on a larger and small substrate of Ag(111). Fig. 5 shows the calculation model and computed image of α-sheet borophene, which shows that the electron density was distributed on two different substrates.[66] Borophene has a monolayer and rectangular structure that allows it to exhibit anisotropic ultimate strengths, whereas the critical strains in the other side hexagonal structure of graphene and silicene are slightly anisotropic in the mechanical properties.[67] Borophene (hydrogenated borophene) has a buckled structure with a buckling height of 0.81 Å, which is lower than that of the borophenes (0.91 Å). The optimized lattice constants are in the *a*- and *b*-directions, which agreed well with previous theoretical results.[68] The structural characteristics of borophene is shown in Table 2.

4.3 Electronic properties

A number of theoretical and experimental studies revealed that boron forms a wide variety of complex structures due to the presence of three electrons in the outer shell. Basically, boron shows a honeycomb structure due to the lack of one electron. A metallic character was noticed in boron because of the half-filled antibonding nature, where it can act as either donor or acceptor property.[69,70] This suggests that borophene could be theoretically developed as a conductor, as well as superconductor. The ionic liquid (IL) shows electromagnetic interaction with electrons on the 2D materials, causing a redistribution of electric charge in both graphene and borophene sheets as a result of the

Table 1 Mechanical properties of borophene

	Elastic stiffness constants					Young's modulus		Poisson ratio		
Phase	C_{11}	C_{22}	C_{12}	C_{66}	C_{44}	Y_a	Y_b	θ_a	θ_b	Ref.
δ3 borophene	73.6	—	11.2	31.3	—	71.9	—	0.152	—	54
δ5 borophene	92.9	—	14.3	36.9	—	90.7	—	0.154	—	
Striped borophene	169.5	—	18.8	35.8	—	167.4	—	0.111	—	
$BH_{1/48}$	250	296.50	14.50	—	104	249.29	295.66	0.049	0.058	55
$BH_{1/8}$	230	235.75	14.63	—	81	229.09	234.82	0.062	0.064	
$BH_{1/2}$	243	219.50	16.50	—	41.50	241.76	218.38	0.075	0.068	
8-*Pmmn* borophene	—	—	—	—	—	241.08	305.20	0.042	0.062	56
h-B_2O	44.13	237.41	65.11	—	11.45	26.27	141.35	0.27	1.48	57
h-B_2H_2	97.63	140.99	31.77	—	13.83	90.47	130.65	0.23	0.33	
2-*Pmmn* borophene	247.1	4.08	106.5	—	525.5	247	106.4	−0.038	−0.016	58
χ3 borophene	198.4	187.6	36.2	63.5	—	187.8	180.8	0.19	0.19	59
β12 borophene	188.1	214.3	36	70.7	—	182.0	207.5	0.17	0.19	
Stripped borophene	382.5	154.2	−5.8	76.4	—	382.3	154.1	−0.04	−0.02	
Borophene (one layer)	396.6	158.4	−3.74	86.5	—	397	158	−0.022	−0.009	60
(Two layer)	380.0	143.8	7.44	75.2	—	380	144	0.052	0.020	
(Three layer)	361.1	141.5	11.29	72.5	—	360	141	0.080	0.031	
(Four layer)	337.9	136.0	12.37	70.8	—	338	136	0.091	0.037	
Borophene	376.6	149.6	−7.64	83.61	—	376.21	149.45	−0.05	−0.02	61
B_4F	275.0	183.6	13.07	79.63	—	274.13	183.04	0.07	0.05	
B_2F	130.1	200.7	6.17	57.35	—	129.93	200.46	0.03	0.05	

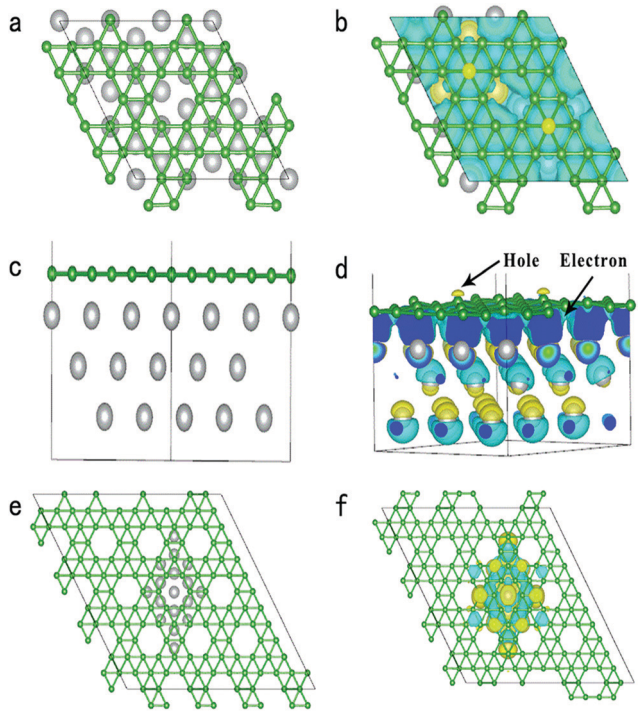

Fig. 5 Few-layer borophene calculation models of a bigger Ag(111) substrate with α-sheet borophene: (a) top view, (b) electron cloud density image, (c) side view, (d) electron distribution density image. Few-layer borophene calculation models of a smaller Ag(111) substrate with α-sheet borophene: (e) top view, (f) electron density distribution image. This figure has been reproduced from ref. 66 with permission from American Chemical Society, copyright 2020.

polarization of the IL, which was based on the Bader analysis and charge density calculations.[71] A DFT study was used to determine the energy and electronic sensitivity of the borophene sheet (B_{36}) toward four nucleobases, in which cytosine has the greatest impact on the borophenes conductivity, facilitating the generation of the greatest electrical signal. Thymine has the second biggest peak, whereas adenine and guanine have the lowest peaks.[72] Anisotropic electronic behaviour is seen in the electronic band structure of the borophene nanosheets (β12, χ3, and striped). Despite the metallic nature of the borophene sheets, applying a directed strain *via* deformation matrices produces a bandgap in certain Brillouin zone areas, allowing mechanical control of the electrical characteristics.[73] Noticeably, the metallic character was found in the in-plane direction of borophene due to the overlapping of the valence and conducting bands, whereas bandgaps increased to 9.43 eV in a zig-zag direction.[69] Borophene exhibited higher superconductivity than MgB_2. Furthermore, the different structures of borophenes (β12, χ3 and δ6) showed different superconductivity values. Similarly, the electronic structures of borophene and g-C_2N were maintained by the borophene/g-C_2N (B/C_2N) vdW heterostructures. The external electric induced the transition between the n-type Schottky contact to the Ohmic contact, and the borophene and g-C_2N carrier concentration interfaces were tuned, as shown in Fig. 6. Researchers calculated the projected band structures of β12 and χ3 B/C_2N with different electric fields.[74] The Landauer–Buttiker formalism was used to conduct a first-principles analysis of the electrical and transport characteristics of borophene and borophane. The DFT calculation demonstrated that borophene has a two-orders-of-magnitude higher electronic current than borophane.[75] At ambient

Table 2 Calculated lattice constants (*a*, *b*) and buckling height (*h*)

Phase	*a* (Å)	*b* (Å)	*h*	Ref.
Borophene	1.617	2.872	—	63
Borophene	1.6	1.8	0.23	64
α′-Boron sheet	4.37	0.173	—	65
Borophene	1.614	2.866	0.911	67
Borophane	1.941	2.815	0.81	68

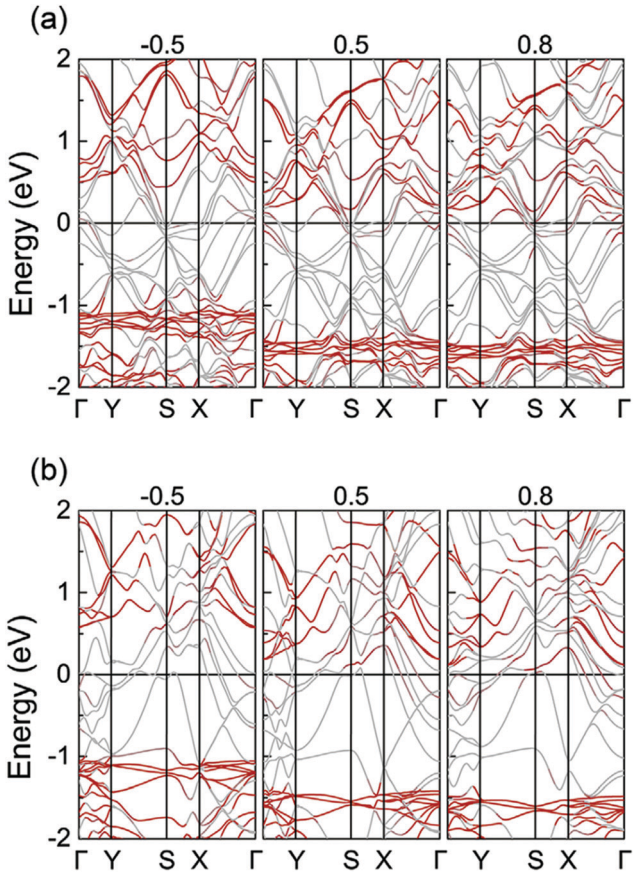

Fig. 6 Different electric fields and band structures of the β12 B/C_2N (a) and χ3 B/C_2N (b) vdW heterostructures. The contributions of borophene and C_2N are shown by grey and red symbols, respectively. The Fermi level is zero. This figure has been reproduced from ref. 74 with permission from Elsevier, copyright 2018.

temperature, borophene shows high thermal conductivity values of 293 and 335 W m K^{-1} in armchair and zigzag directions.[76]

4.4 Optical properties

The computational optical characteristics revealed that the static dielectric constant of borophene was increased by the doping of Al and Ga metals into borophene, which improved the borophene capacity to store electromagnetic energy. After doping, the peak reflectivity fell and the static refractive index rose, filling the gap in the borophene materials, which led to the absorption of red and infrared light.[77] The optical characteristics of borophene were significantly changed as the incoming light direction changed. Meanwhile, in the borophene sheet and perpendicular light angles, the metallic and semiconductor behaviour changed. As a result, the optical characteristics of this material may be described as anisotropic.[78]

Experimental data demonstrated that the optical response of borophene could be adjusted by applying a tensile/compressive strain and coating the borophene surface with hydrogen and fluorine atoms.[79] The goal of this research was to look into the nonlinear optical characteristics of borophene modified with superhalogen, and the absorption characteristics of pure and borophene modified with superhalogen were studied in the UV-Vis-NIR region.[80] The optical conductivity of different structures of borophene (χ3-borophene single layer, zigzag, armchair and BNTs, zigzag, and armchair nanoribbons) should be investigated before looking at the optical transmission and reflection. Fig. 7 describes the definite portion of the optical conductivity, transmission, and reflection of these structures. Polarization periodic directions were examined, as well as the inter-band and intra-band contributions.[81] Overall, borophene exhibited good optical properties. Furthermore, 2D boron polymorphs (borophene) exhibited a metallic nature with high free charge carrier concentration. It favored exhibiting plasmonic properties in the visible range of frequencies, which suggests that borophene is the first material with high frequency 2D plasmons.[82] Large-scale hydrogenated borophenes have been synthesized by a three-step heating process *via in situ* thermal decomposition of $NaBH_4$ without any metal substrates.[43] Spectroscopic techniques (UV-Vis and photoluminescence (PL)) were used to measure the optical properties of borophenes. The UV-Vis and PL spectra show the similar energy (2.49 eV) in hydrogenated borophenes.[43]

4.5. Thermal conductivity

Computational theories, such as molecular dynamic (MD) simulations, density function perturbation theory (DFPT), non-equilibrium Green function (NEGF) and the Boltzmann transport equation (pBTE), have been used for the determination of the thermal conductivity of borophene.[69,70] It was noticed that the β12 and χ3 structures of borophene showed different thermal properties (conductivity and thermal stability). For example, δ6 borophene exhibited thermal conductivity values of 22.6 × 10^{-9} and ∼43.3 × 10^{-9} in the zig-zag and armchair directions, respectively, at ambient conditions. These values are lower than that for graphene (1775 × 10^{-9} W K^{-1}), illustrating that the thermal stability of borophene is lower than that for graphene. Furthermore, borophene showed a thermal conductivity nature that was strongly dependent on the structure of borophene, where borophene was successfully used in the thermal insulation and thermoelectric industries (lower thermal conductivity borophne), and in the fabrication of photovoltaic and electronic devices (high thermal conductivity borophene).

4.6. Magnetic properties

Spin-polarized DFT calculations were demonstrated for the estimation of the magnetic nature of borophene.[83] The DFT calculations illustrated that the 1d quasi planar borophene has a ferromagnetic nature. Another study used first-principles calculations for the determination of the magnetic and electronic properties of the 3d transition metal atom-functionalized borophene.[84] These data demonstrated that the 3d transition metal atoms (Ti, Mn, V, Cr, and Fe) were effectively adsorbed on the surface of borophene with greater binding energies (5.9 and 8.3 eV), favoring a change of the nonmagnetic nature to a ferromagnetic nature in borophene. These theoretical studies illustrated that borophene could be used as a promising material in electronics and spintronics research areas.

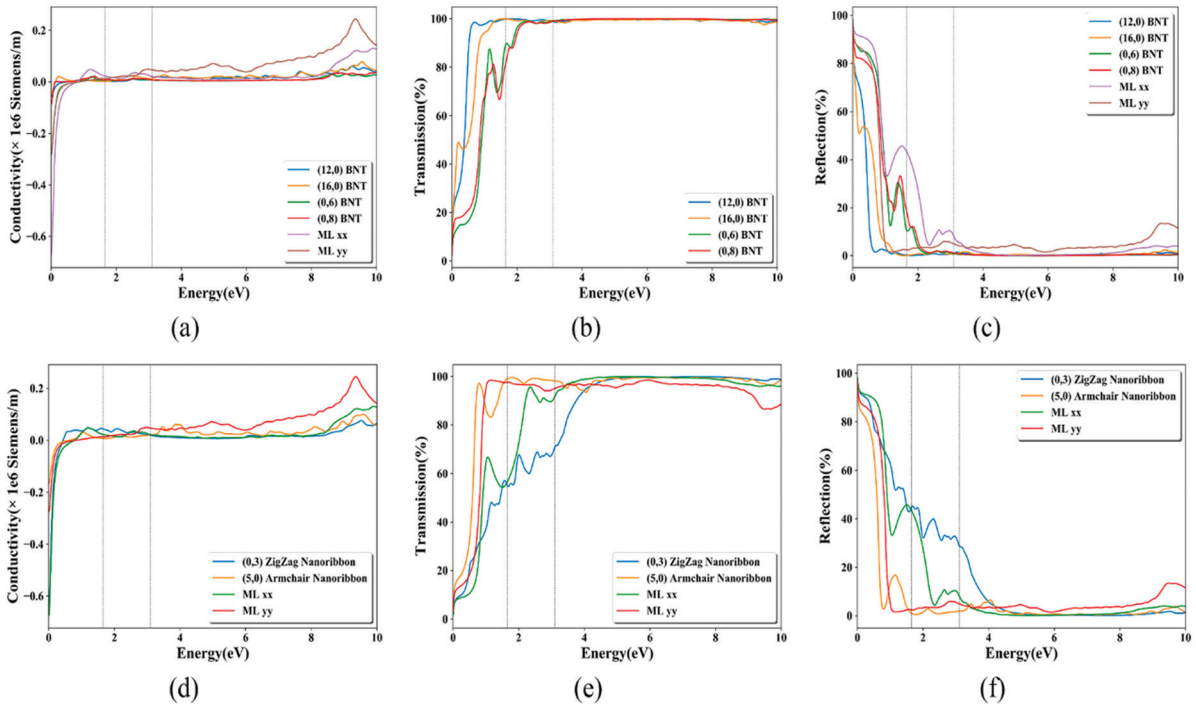

Fig. 7 (a and d) Optical conductivity (%), (b and e) transmission (%), and (c and f) reflection (%) of different structures of borophene. This figure has been reproduced from ref. 81 with permission from Elsevier, copyright 2021.

5. Applications of borophene

In recent years, borophene nanostructures have evolved as a novel class of 2D nanomaterials in various fields because of its similarities with the graphene structure. This section describes the applications of borophene in the sensing of various chemicals, and in the fabrication of batteries and storage devices.

5.1. Sensing applications

2D Materials act as promising materials in the sensing of gas molecules with ultra-sensitivity because of their thinness. This research explores and estimates the effect that decorating boron with the Na atom has on adsorbing CO and CO_2 molecules using DFT calculations. Generally, CO/CO_2 molecules have higher adsorption energies, which allows borophene to be a better adsorbent and potential alternative for the capturing and sensing of gas molecules. The adsorption energy of the CO and CO_2 molecules are 1.895 eV or −0.490 eV when they are attached to the surface of borophene. The current increases linearly from 0.0 to 1.4 V with increasing adsorption rates of CO/CO_2 molecules. Because Na-decorated borophene monolayers are sensitive to CO and CO_2, sensors that utilize these materials to detect these gases in the environment are feasible.[85]

DFT calculations were performed to estimate the adsorption energies of several gases on the borophene/MoS_2 heterostructure.[86] The other four compounds (except CO_2) bind with borophene. It may be termed physisorption due to the little interaction between borophene and the CO_2 molecule. In this approach, the transport properties of borophene were studied by the non-equilibrium Green's function (NEGF) method, demonstrating that heterostructures of borophene are inclined toward the NO molecule.[86] Furthermore, the DFT calculations were utilized for the first time to create a novel, sensitive, selective and reproductive formaldehyde sensor, in which β12-borophene sheets were functionalized with SnO_2.[87] This study demonstrated that the zero-band-gap β12-borophene alloy with a moderate direct gap (1.09 eV) was mixed with the SnO_2 semiconductor (wide direct gap) to create a hybrid heterostructure that resulted in several features, such as long-term stability, selectivity, electrical conductivity and HCHO molecule response. The electrical conductivity of the borophene/HCHO@β12-borophene/SnO_2 systems was significantly increased by the chemisorption (1.81–4.19 eV) with good adsorption energies, which resulted in a lower band gap energy. As a consequence, the HCHO adsorption was almost entirely dependent on the molecular structure of the β12-borophene/SnO_2 system.

Using semiconducting 2H-MoS_2 as the substrate, scientists hypothesized that they could theoretically fabricate the borophene and MoS_2 heterostructure *via* vdW interactions, resulting in the evaluation of the transport and sensing abilities towards organic molecules. According to DFT, the CH_4, C_2H_4, or CH_3OH interactions are quite weak since borophenes exhibited strong chemical interactions with the above molecules, leading to strong chemisorption, which favors the use of borophene as a promising adsorbent for C_2H_2 and HCHO molecules. The sp^3 hybridization of the C atoms in both organic molecules is induced by C_2H_2 and HCHO, which results in the chemisorption reaction. The heterostructure's sensing performance is very anisotropic and highly

sensitive to C_2H_2 and HCHO, which was confirmed by NEGF method.[88]

Fig. 8 illustrates the total density of state (DOS) of borophene and partial density of state (PDOS) on the line defects alone and line defects with NO, NO_2, and NH_3 gas adsorption, respectively. The author demonstrated that β12 and χ3 borophenes possess intrinsic line defects. The DFT simulation study was carried out on the adsorption abilities of the N-containing gas molecules on borophene.[89] For sensing inorganic small molecules in the environment, borophene was modified with MoS_2 for the sensing of the gas (NH_3) molecule due to its high anisotropic properties. The transport characteristics of the β12 borophene on the MoS_2 substrate for gas sensing were investigated using the NEGF technique. The gas sensing capability of β12 borophene was found to be extremely anisotropic, particularly for NH_3, which has the highest anisotropic gas sensing ratio of 17.43.[90]

To investigate the gas sensing ability, a χ3-borophene nanoribbon was put between two χ3-borophene nanoribbon electrodes and their sensing ability was studied by NEGF and DFT methods.[91] When compared to NO and water vapor, the sensor showed a high degree of selectivity for H_2S. With the high adsorption energies, there is a large transfer of charge from the molecules to the ribbon's edges. The 2D borophene was fabricated with buckling and line-defective phases, and studied for the adsorption of CO, NO_2, NO, and NH_3 gas molecules.[92] It was found that the adsorption energy of borophene is large, and it generates distinctive creases. To calculate the materials transport characteristics, the NFGF method was employed.[92] This proves that borophene is an excellent gas sensor. The adsorption geometry and the adsorption position of the adenine molecule on the surface of the borophene sheet were discovered to vary with direction.[93] The proper placement and direction of the adenine molecule on the borophene surface had an effect on the compound's selectivity and sensitivity. Borophene is an excellent choice to use as a sensor for nucleotide detection due to its high adsorption energies and

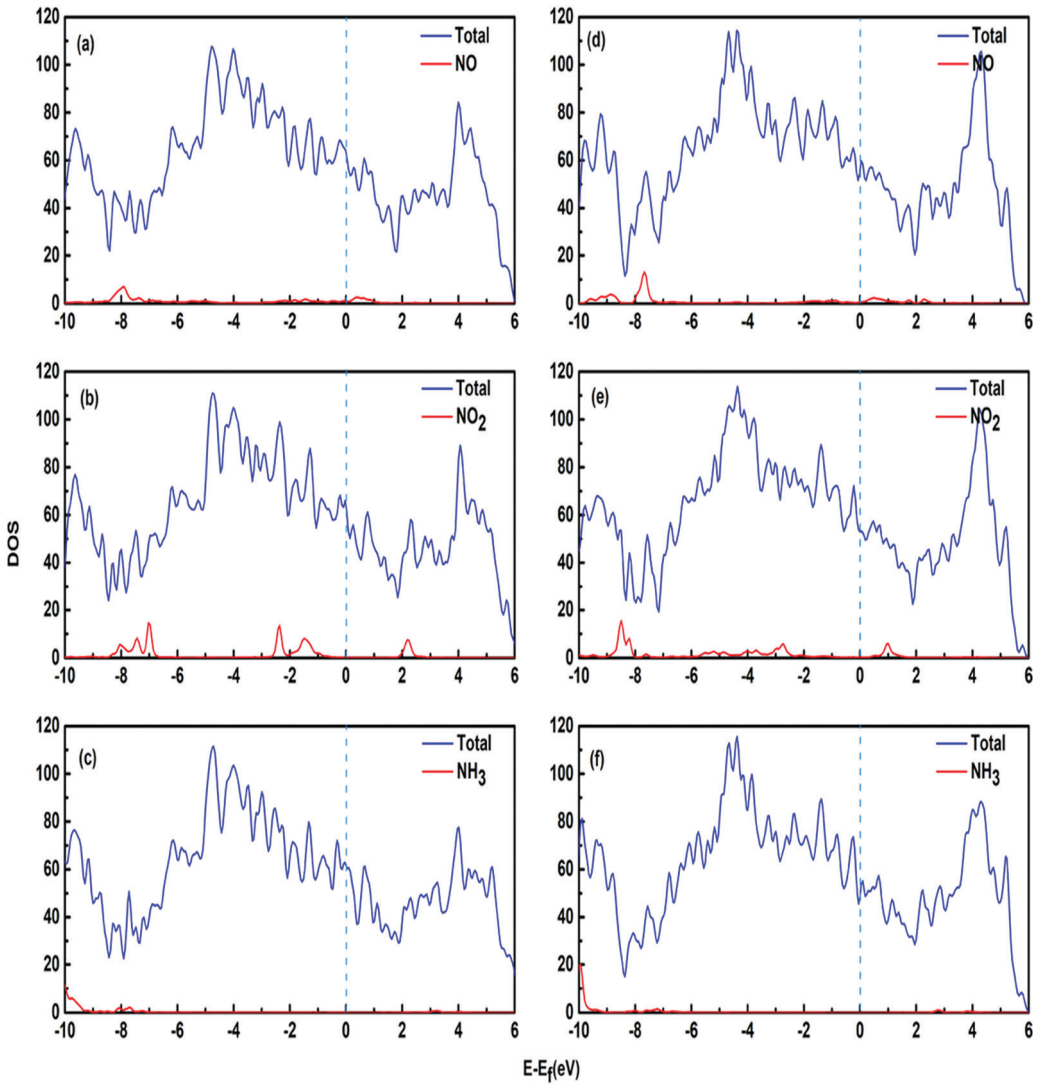

Fig. 8 For β12 borophene and χ3 borophene, the total DOS with gas adsorption on the line defects (blue lines) and PDOS from the gas molecule (red lines). This figure has been reproduced from ref. 89 with permission from American Chemical Society, copyright 2020.

strong charge transfer. The authors noticed physico-chemical interactions between adenine and borophene, signifying that borophene could be used as a promising material for the sensing of nucleic acids.

To obtain a fully comprehensive understanding of borophenes' adsorption ability and capacity onto SO_2, adsorption studies were performed for one molecule and up to eight molecules. The results showed that borophene showed excellent adsorption ability and capacity towards SO_2 molecules, with up to seven molecules being adsorbed on its surface *via* chemisorption. This was estimated using the relaxed adsorption configuration and large values of E_{ad} and (charge transfer) Q_T.[94] The interactions of β12 borophene with five hazardous gases, namely CO, NO, NH_3, NO_2, and CO_2, were studied using non-empirical vdW density functionals to provide insight into the borophenes adsorption behavior.[95] Other gases are chemically linked to β12 borophene, whereas CO_2 is adsorbed *via* physisorption. Furthermore, they highlighted the importance of β12 borophene deformation, particularly in the instances of CO and NH_3 adsorption. According to the findings, the adsorption energies and charge transfers, borophene is the most sensitive to NO_2 gas and the least susceptible to CO_2.

Using the NEGF and DFT techniques, the electrical and chemical features of borophene nanotubes (BNTs) were examined using trimethyl amine (TMA) and dimethyl amine (DMA) molecules, and its adsorption ability towards TMA and DMA were studied.[96] In the device density of states spectrum, the peak maxima shift shows that there is an electron transfer between BNT and the target molecules (TMA and DMA). The bandgap of BNTs is 0.34 eV. The current varies from 10^{-11} to 10^{-6} A in the BNTs device, which is proportional to the quantity of TMA and DMA. Pristine borophenes exhibited semi-metallic properties because of its energy bandgap. For investigating the interactions of NH_3 molecules with borophene, several studies including the adsorption energy, Bader charge transfer, energy band gap and density-of-states spectrum were studied. Borophene was found to be an efficient material to adsorb NH_3 gas on the surface of borophene.[97] Furthermore, the investigation illustrated that the hazardous NH_3 gas molecules can interact with borophene nanosheets and nanotubes at the atomic level. A typical isolated borophene nanosheet has a band gap of 0.32 eV, whereas a typical isolated borophene nanotube has a band gap of 0.22 eV.[97]

Recently, the B_{36} nanosheet was computationally designed with a planar C_{6V} structure that has a central hexagonal hole.[98] The structural features of the B_{36} borophene nanosheet were successfully demonstrated for the detection of HCN, exhibiting strong physical and chemisorption, which showed remarkable changes in the electronic properties of borophene (B_{36}). The electronic structure of borophene (B_{36}) was significantly influenced by the adsorption of HCN. Furthermore, borophene nanosheets with the β_{12} phase crystalline nature were successfully produced *via* ultrasonication, and the prepared borophene nanosheets were functionalized with polyaniline for the electrochemical sensing of glucose.[99] The authors investigated the stability of the prepared borophene by the zeta potential, showing that the prepared β_{12} borophene nanosheets exhibited electrostatic repulsion, which is good enough to confirm the stability of borophene. Furthermore, the zeta potential of the β_{12} borophene nanosheets with polyaniline showed negative charge density, favoring an increase in the conductivity of borophene–polyaniline, which is higher than polyaniline. These changes play a key role in exploring borophene as a promising material for the modification of electrodes, which offers a high degree of charge transfer mechanism. Thus, the borophene–polyaniline-based electrochemical sensor was developed for sensing of glucose, showing the limit of detection at 0.5 mM. The synthesis of stable borophene was successfully completed, and it was used as a promising material for the fabrication of 2D heterostructures.[100] Borophene–graphene heterostructure nanomaterials have been synthesized by heating the mixture of $NaBH_4$ and few-layered graphene. The as-prepared borophene–graphene heterostructure acted as a humidity sensor, exhibiting several analytical features, including rapid response, ultrahigh sensitivity, and stability (Fig. 9). Importantly, the fabricated 2D borophene–graphene-based sensor exhibited ~700 times higher sensitivity than pristine graphene, and superior sensitivity among all 2D materials-based sensors. Similarly, the p–n junction of the borophene–MoS_2 heterostructure has been theoretically predicted as a potential candidate for ultrahigh humidity sensing applications.[101] The as-prepared heterostructure humidity sensor showed good sensing characteristics (high sensitivity, rapidity, good stability, selectivity and good flexibility), exhibiting higher sensitivity (15 500%) at a relative humidity (RH) of 97%, which indicates that the borophene–MoS_2 heterostructure humidity sensor is 70 or 90 times higher than that of MoS_2 or borophene as humidity sensors. The fabricated borophene–MoS_2 heterostructure humidity sensor exhibited outstanding selectivity towards water vapor as compared to organic vapors, demonstrating its potential applications in the development of a human breath diagnosis system.

Recently, first-principles calculations have successfully demonstrated borophene as a promising material for gas sensing applications, specifically for NO_2 gas.[102] It was noticed that the borophene-based chemiresistive sensor exhibited a wider linear range from 200 ppb to 100 ppm, offering several analytical merits such as lower detection limit (200 ppb), rapid response (30 s), and good recovery (200 s) at room temperature. The developed borophene-based sensor exhibited flexibility, stability and selectivity for the sensing of NO_2 gas (Fig. 10). Additional first-principles calculations successfully demonstrated the growth of Ag(111)-supported borophene *via* oxidation method of the free-standing and DFT calculations.[103] In this instance, a triplet to singlet transition of O_2 molecule may occur, followed by the barrierless oxidation method in the case of the free-standing and Ag(111)-supported borophene. The authors demonstrated a significant net charge transfer from the metal surface (Ag(111)) to the single layer of borophene. It was also observed that a triplet-to-singlet transition takes place only with the Ag(111)-supported borophene, which does not happen in the presence of the metal surface (Ag(111) alone. Comprehensive studies based on DFT calculations showed that O_2 molecules are easily chemisorbed on the supported β12-borophene and disintegrate into individual

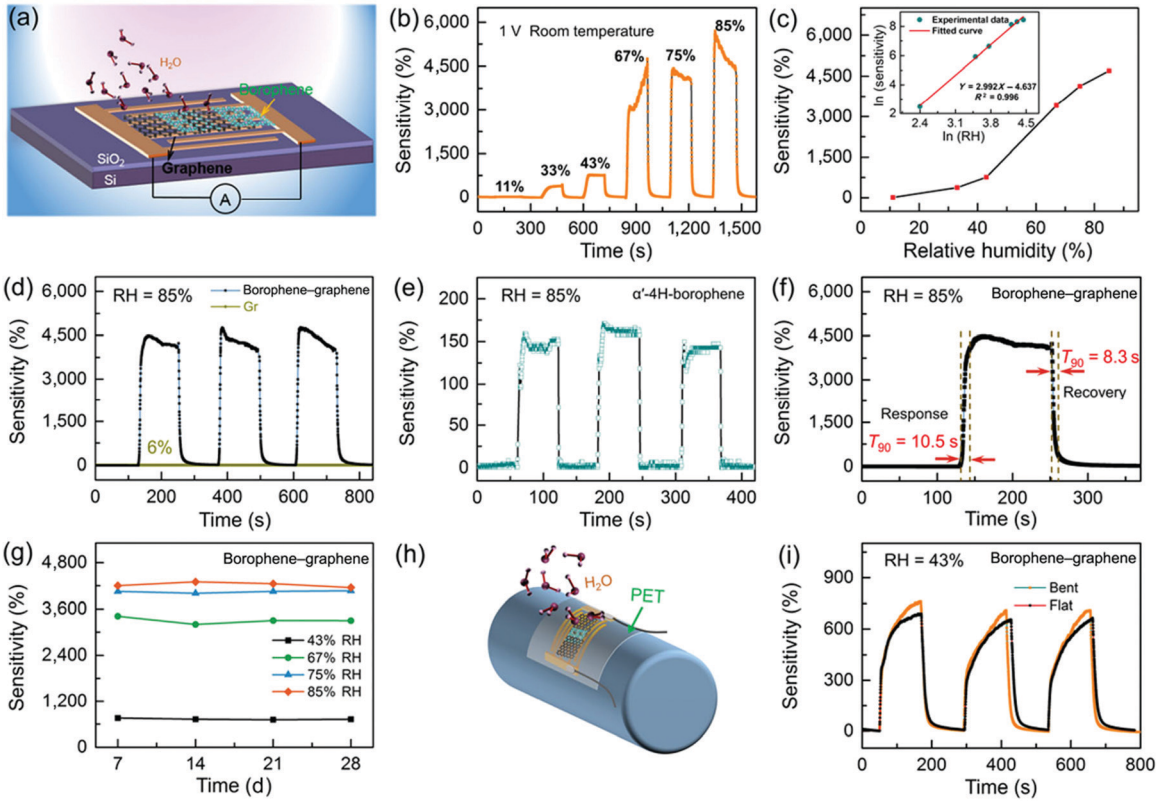

Fig. 9 Fabrication of a borophene–graphene humidity sensor. (a) Schematic representation of the borophene–graphene-based humidity sensor. (b) Switching the RH humidity sensing behaviour of the heterostructure sensor. (c) Variation in the RH levels of the heterostructure sensor sensitivity. (d and e) Repeatability of the borophene–graphene heterostructure humidity sensor at 85%. (f) Investigation of the recovery and response curve of the heterostructure sensor at 85% RH. (g) Stability of the borophene–graphene heterostructure sensor. (h) The borophene–graphene heterostructure humidity sensor on a PET substrate. (i) Response curves of sensing with and without bending strain. This figure has been reproduced from ref. 100 with permission from Springer Nature, copyright 2021.

atoms by removing the barriers and spin triplet-to-singlet conversion, which is not important in the chemical absorption process. A comparison of their estimated core-level binding energies with the experimental XPS spectroscopic results demonstrated that the boron atoms are very active in the supported borophenes, instead of being inert to oxidation.[104] These results revealed that borophene could be used as a potential material for the development of sensing devices with remarkable selectivity and sensitivity. Table 3 provides an overview the potential applications of borophene nanomaterials for the sensing of various molecules.

5.2. Applications in batteries

Recent studies revealed that χ3-borophene has proven to be a potential 2D anode material for LIBs. However, its pristine structure must be improved in order to boost its specific capacity and Li diffusivity. The DFT model was utilized to investigate the χ3 fluorine decoration in order to achieve this goal.[105] The structures Fχ3-A and Fχ3-B were found to have very comparable energies and good kinetic stability. These studies showed that during the whole lithiation process, there was good metallic property on the surface. Fig. 11 shows the theoretical specific capacity and open circuit voltage (OCV) of Li_{10}Fχ3-B.[95] In high performance, the (lithium–sulfur (Li–S) batteries showed the ''shuttle effect'' that restricts the performance of the battery due to the movement of the polysulfide molecules. The Li–S batteries may be improved by creating catalytic materials that entrap and immobilize the polysulfides. Low-lithiation structures with covalent B–B and metallic Mo–Mo bonds offer active sites for polysulfide anchoring, while MoB_2 also possesses a high conductivity that speeds up the polysulfide conversion.[106] The interactions of the stripes (β_{12}) and honeycombs (Hb) forms of borophene with lithium ions were investigated. The adsorption energies calculated for the two electrodes are −1.720 and 0.512 eV, respectively.[107] Hexagonal borophene nanosheets are kinetically unstable due to the electrons of the π-valence orbitals of the hexagonal borophene nanosheets. The Wu group theoretically described the Fe atom functionalized borophene (FeB_6), where the Fe atom is located at the center of the partial boron rings.[108] The authors explored the potential use of the FeB_6 single layer nanosheets as an anode material for NIBs and LiBs. The designed FeB_6 nanosheet exhibited strong adsorption energies at 2.39 and 2.89 eV for Na and Li, respectively. Using these materials, low diffusion barriers were noticed at 0.10 and 0.24 eV for Na and Li, respectively. These observations revealed that FeB_6 nanosheets could be used as promising anode materials for NIBs and LIBs.

Some of the properties (thermal mechanical and stability) of borophene were greatly improved by designing 3D two metallic

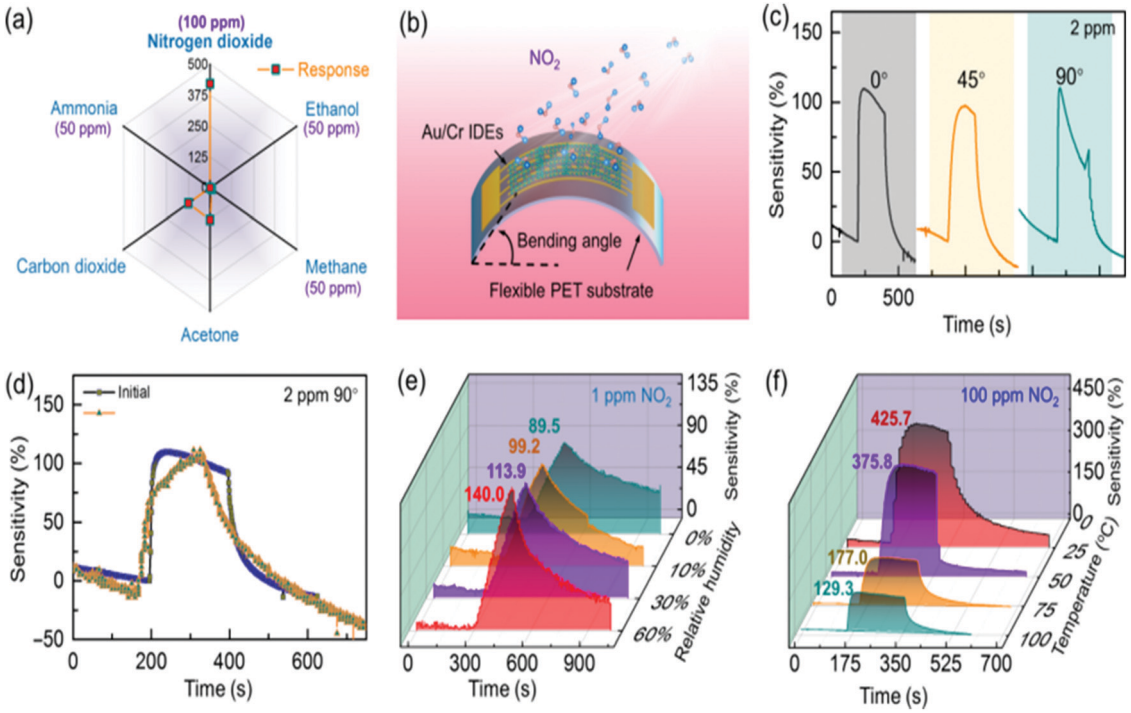

Fig. 10 Development of a borophene sensor (selectivity, flexibility and stability). (a) Investigation of the selectivity of the borophene sensor with different gases. (b) Schematic diagram of the borophene sensor on flexible PET at the bending state. (c) Response curves of the real time analysis. Response of the NO_2 sensor at (d) room temperature and (e) at different temperatures in NO_2. This figure has been reproduced from ref. 102 with permission from Springer Nature, copyright 2021.

borophene.[109] It was observed that B px-orbitals greatly influence metallicity. The authors noticed that the Li^+, Na^+ and K^+-based 3D-β_{12}-borophene acted as promising anode materials with remarkable features, such as small volume changes, ultrahigh capacities, appropriate average open-circuit voltages and low migration energy barriers, respectively. The trend of adsorption energies with increasing Na concentration and most stable adsorption sites were investigated for the Na atom adsorptions on β12–χ3–β12 and χ3–β12–χ3.[110] The findings showed that the adsorption of Na and the metallic behaviour of both phases remain constant.[110] By combining blue phosphorene (BP) and borophene monolayers, a new BP/borophene heterostructure was created.[111] The pristine BP monolayer has a semiconductor property, while BP/borophene has a metallic character. The BP/borophene heterostructure may be an ideal option as an anode material for LIBs because of these characteristics, which offer enormous electrical conductivity, high capacity, low diffusive energy barriers and adsorption energies.

A new graphene-like HBS oxide (h-B_3O) is created by replacing partial boron atoms in an HBS with O_2 atoms. The thermal stability of h-B_3O was confirmed by molecular dynamics simulations.[112] In this instance, first-principles calculations were used to study the potential of the h-B_3O monolayers anodes for LIBs and NIBs.[112] When compared to pristine borophene, the electrical characteristics of the lithiated- and delithiated-borophene showed metallic behaviour, while the mechanical stiffness of the interface rose threefold.[113] The low ion-transport barrier and high metallic conductivity of developed borophene showed excellent Li-storage capacity. The Li-storage capacity of B/MoS_2 is 539 mA h g^{-1}, which is lower than that of earlier models because of its weaker ion-hopping barriers.[114] To round up the collection of 2D materials, buckled and flat borophene nanomembranes have just been introduced. Four different flat borophene films, using first-principles DFT simulations, were studied as future anode materials for batteries.[115] These simulation studies revealed that Mg, Na, or Li-IBs with very high capacity anode materials are generated by using flat borophene sheets.[115]

According to the DFT calculations and first-principles molecular dynamics simulations, borophene possesses several interesting characteristics, including ultrahigh energy storage and rapid ion transport in metal ion batteries.[116] For both LIBs and NIBs, the newly discovered borophene (2D boron sheet) may be a suitable electrode material with excellent electrochemical performance. The computation studies are carried out on β12 and χ3 borophene structures, demonstrating that both structures are empirically stable. Similarly, first-principles DFT simulations successfully explored the four different flat borophene nanostructure materials as an anode for the development of Mg, Al, Li and Na-ion batteries.[117] These studies demonstrated that flat borophene films exhibited the thermally stable and electrically conductive nature with ultrahigh capacities of 2040, 1640 and 2480 mA h g^{-1} for the Li, Na and Mg-ion batteries, respectively. These theoretical data illustrated that borophene could be used as a promising material

Table 3 Sensing applications of borophene

Species	Computational method	Sensing molecule	Mechanism	Adsorption energy (eV)	Ref.
Na-decorated borophene	DFT	CO and CO_2	—	–1.895 –0.490	85
Borophene/MoS_2 heterostructure	DFT and NEGF	CO, CO_2, NO, NO_2 and NH_3	Chemisorption and physisorption	−1.15 −0.64 −1.47 −2.12 −1.52	86
SnO_2/β12-borophene	DFT	HCHO	Chemisorption	−1.81	87
Borophene/MoS_2	NEGF	CH_4, C_2H_4, C_2H_2, CH_3OH, and HCHO	Chemisorption and physisorption	−0.17 −0.32 −0.41 −3.06 −2.57	88
β12 borophenes	DFT and NEGF	NO, NO_2, and NH_3	—	−1.13 −1.89 −2.20	89
χ3 borophenes	DFT and NEGF	NH_3, NO_2, and NO		−1.48 −2.14 −1.93	
β12 borophene/MoS_2	NEGF	CO, NO, NO_2, and NH_3	Chemisorption	0.99 0.81 1.63 0.62	90
χ3-borophene nanoribbon	DFT and NEGF	H_2S	—	−5.35	91
Buckled borophene	NEGF	NH_3, NO, NO_2, and CO	—	1.45 1.08 1.75 1.24	92
line-defective borophene	NEGF	NH_3, NO, NO_2, and CO	—	1.11 0.95 1.80 1.19	
Borophene sheet	DFT	Adenine	—	− 2.09	93
borophene	DFT	SO_2	Chemisorption	− 3.178	94
β12 borophene	DFT	CO, NO, NH_3, NO_2, and CO_2	Chemisorption	−0.49 −0.38 −0.41 −1.28 −0.19	95
Borophene nanotube	NEGF and DFT	DMA and TMA	—	−1.015 −0.780	96
BNS	DFT	NH_3	—	−1.951	97
BNT	DFT	NH_3		−3.742	
B_{36} borophene nanosheet	DFT	HCN	Chemisorption	0.19	98
PANI:β12 borophene	—	Glucose	Electrochemical	—	99

DFT = density functional theory, NEFG = non-equilibrium Green's function, DMA = dimethyl amine, TMA = trimethyl amine, BNS = borophene nanosheet, BNT = borophene nanotubes.

for the fabrication of lightweight rechargeable ion batteries with high capacity. Additional DFT and first-principles molecular dynamics simulations were described for the use of borophene as an anode material in different metal (Al, Mg, K, Na and Li) ion batteries.[118] The designed borophene nanostructure showed higher specific density and high charging voltage values, suggesting that borophene nanosheets could be used as a promising anode material in the development of ion batteries. To explore the potential of borophene as an anode material for LIBs, another study described the use of *ab initio* molecular dynamics simulations for ion batteries.[119] The adsorption energy is −1.12 eV for the lithium atom in borophene, which is substantial enough to guarantee excellent lithium–borophene stability throughout the lithiation process.

For LIBs and NIBs, the storage capacities of β12 and borophene are 1984 1240 mA h g^{-1}, which are greater than that for the graphite electrode.[120] The ultra-high capacity in LIBs and NIBs was also shown by 2D honeycomb borophene oxide (h-B_2O).[121] Furthermore, 2D h-B_2O exhibits excellent conductivity, a low Li/Na diffusion barrier, a low average open-circuit voltage, and modest lattice change characteristics before and after Li/Na adsorption.[121] The storage capacity of borophene nanosheet was noticed as 433 mA h g^{-1} for Zn–ion batteries, illustrating its characteristic features such as low average intercalation voltages and minimal diffusion energy barriers for the ion batteries.[122] Calculations on semiconducting borophene indicated that it has not only higher Li/Na adsorption energies, but it exhibited a large Li/Na capacity.[123] The possibility of the 2D hydrogen boride nanosheet as an anode material in

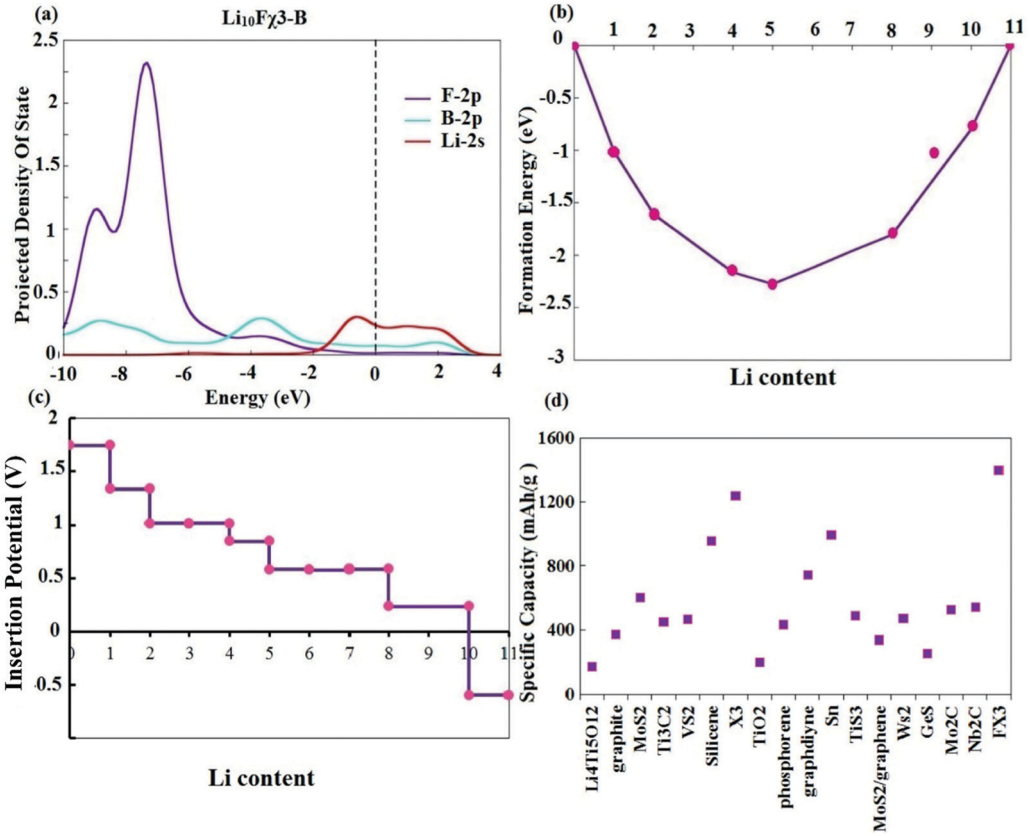

Fig. 11 (a) The PDOS of $Li_{10}F\chi3$-B, (b) the formation energy of LixFχ3-B, (c) OCV profile *versus* Li content in LixFχ3-B, and (d) the theoretical specific capacities of some common 2D anode materials compared to that of Fχ3-B. This figure has been reproduced from ref. 105 with permission from Elsevier, copyright 2020.

Li/Na IBs was studied.[124] It was noticed that the Na atoms showed a strong ability to adsorb onto the borophene with a binding energy of about −1.48 eV for hexagonal vacancies in the B layer and −1.731 eV for the close-packed triangular B layer.[125] They predicted a series of stable MgB_x with broad stoichiometries in the range of $2 < x < 16$ by eliminating Mg atoms from MgB_2. As the charge transfer was altered by the Mg injection and extraction, the process can be switched back and forth. The flexible valence state of boron in its planar form is responsible for the mechanism of such a charge-driven change.[126] The applications of borophene in batteries are summarized in Table 4.

5.3. Hydrogen storage applications

Recently, hydrogen has been recognized as one of the important sources for the development of clean energy devices because of its safety, compactness and cost-effectiveness.[70] In view of this, borophene has sparked a lot of attention among post-graphene 2D materials.[69,70] For example, the H_2 storage capacity of confined Li-ion functionalized borophene nanosheets was demonstrated using vdW-corrected DFT and a quantum thermodynamic model.[127] Three kinds of Ca-decorated borophene (S1, S2 and S3) were recently synthesized, and their application for H_2 storage characteristics was studied. It was observed that S2 and S3 were found to be potential materials for high-capacity H_2 storage, exhibiting gravimetric H_2 densities of 9.5 wt% and 7.2 wt%, respectively, whereas S1 showed poor values. In the adsorption of H_2, both the polarization and orbital hybridization mechanisms are implicated.[128]

Furthermore, the DFT calculations were used for the estimation of alkali metal-borophene for hydrogen storage applications.[129] The authors observed that alkali metals-borophene showed higher adsorption ability towards H_2 gas. The binding energy of Ca, Na and Li-decorated borophene was increased towards the single H_2 molecule over the undecorated borophene. Recently, systematic theoretical models were illustrated on the decoration of Ti atoms on the surface of the borophene nanosheets ($B_{16}Ti_4$) for hydrogen storage applications.[130] These models confirmed that the hydrogen storage capacity of borophene was greatly enhanced by decorating Ti atoms on borophene, thereby offering the ability to bind 8 H_2 molecules on each Ti atom in the Ti-decorated borophene ($B_{16}Ti_4$). As a result, Ti atoms on the surface of the borophene nanosheet increased the H_2 storage, and the Ti atoms tended to be scattered over the χ3 borophene because of the energy barrier greater than 1.15 eV, which prohibited Ti atoms from the aggregation.[130]

In order to examine the hydrogen storage capacity in the heteroatom-doped borophene, N-decorated and inserted borophene nanosheets were designed. Their H_2 storage capacity was studied by first-principles calculations based on DFT.[131] A strong connection is formed between the N atom and the borophene sheet, preventing it from clustering. N-decorated and

Table 4 Applications of borophene in batteries

Anode material	Capacity (mA h g^{-1})	Adsorption energy (eV)/ diffusion barrier	Storage device	Ref.
$Li_{10}F\chi3$-B	1396	−1.75	Li	105
Li_2S_6-based MoB_2	1116	—	Li	106
β12-lithium ion	929	−1.710	Li	107
Hb-lithium	584	−0.517	Li	
FeB_6	991	2.89	Li	108
	622	2.39	Na	
3D-β12	1653	0.55	Li	109
borophene	1239	0.25	Na	
	619	0.23	K	
3D-B_7P_2	1363	0.23	Li	
	993	0.13	Na	
	681	0.05	K	
β12–χ3–β12	1264	0.22	Na	110
χ3–β12–χ3	1536	0.24	Na	
BP/borophene	1019	0.30	Li	111
$P_{0.5}BLi_x$				
B/G	1469.35	−2.959	Li	112
HB	1134	−2.32	Li	113
	1134	−1.27	Na	
h-B_3O	1161	−2.33	Li	114
	375	−1.70	Na	
B/BN	1698	—	Li	115
B/MoS_2	539	−1.35	Li	116
Borophene films	2480	0.517	Mg	117
	1640	−0.786	Na	
	2040	−1.054	Li	
Borophene	3306	1.46	Li	118
$Li_{0.75}B$	1860	−1.12	Li	119
β12 borophene	1984	−1.046	Li	120
		−1.027	Na	
χ3 borophene	1240	−0.803	Li	
		−0.878	Li	
$B_{18}O_9Li$	2137	< 0.5	Li	121
$B_{18}O_9Na$	1425		Na	
Borophene	433	0.79	Zn	122
Semiconducting	1239.56	−1.62	Li	123
borophene		−1.41	Na	
HB	861.78	−1.0	Li	124
		−0.56	Na	
$Na_{0.083}B$	248	−1.731	Na	125
$Na_{0.1}B$	298	−1.448		

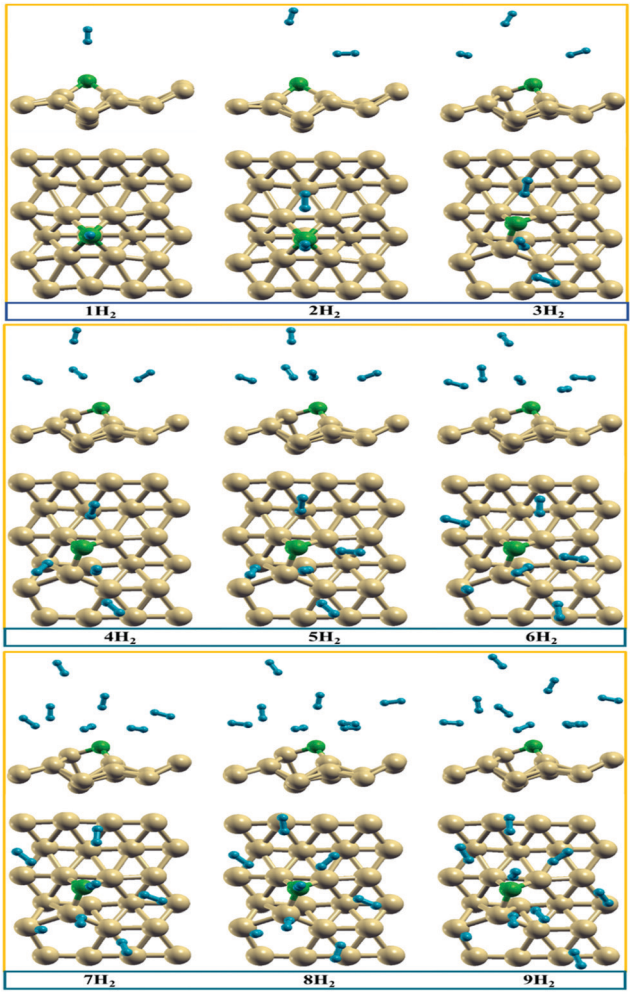

Fig. 12 H_2 molecules adsorbed on an N-decorated borophene sheet in optimized configurations. This figure has been reproduced from ref. 131 with permission from Elsevier, copyright 2020.

borophene sheets have a gravimetric density of good percent correspondingly for H_2 storage. Fig. 12 represents the optimized configurations of nH_2 molecules adsorbed over the N-decorated borophene nanosheet.[131] In addition, three types of borophene nanosheets were fabricated by doping three alkali-metals (K, Na and Li) on the Ag substrate.[132] A strong binding strength was noticed between borophene and alkali–metal atoms and borophene, favoring the generation of metal nanoclusters, which avoids the aggregation of metal nanoclusters and borophene.

Pristine β12- and Li-decorated β12-borophenes were systematically investigated by first-principles calculations based on DFT for their H_2 storage capacity.[133] Among the β12- and Li-decorated β12-borophenes, Li-decorated β12 borophene exhibited higher adsorption capacity towards hydrogen, where the H_2 molecule strongly interacted with the surfaces of the Li-decorated β12 borophene *via* covalent bonding. Numerical data revealed that lithium-β12-borophene has the ability to adsorb up to 7 molecules of H_2. Meanwhile, for the lithium-β12-borophene with H_2, a storage capacity of 10.85 wt% can adsorb up to 14 molecules of H_2. Another theoretical approach was the successful demonstration of the Li atom-decorated β12 and χ3 borophenes for H_2 storage applications.[134] Theoretical investigations demonstrated that the decoration of Li on the surface of borophene offers efficient hydrogen adsorption, thereby facilitating the maximum gravimetric density of H_2 at 10.79 wt% and 8.76 wt% for Li-decorated χ3- and β12 borophenes, respectively. Furthermore, Li-modified borophene was demonstrated as a potential material for hydrogen storage through various theoretical calculations.[135] The Li atoms-modified borophene greatly improved the H_2 adsorption capacity, where the single Li atom is capable of adsorbing three H_2 molecules. However, if the Li atom attached both sides of the borophene nanosheets, the adsorption capacity reached four H_2 molecules. As a result, the H_2 storage capacity is 13.7 wt% with average adsorption energies of 0.142 and 0.176 eV per H_2. According to the PDOS data for Li atoms and H atoms on the Li/borophene nanosheet, the Li atoms and H atoms seem to be embedded in a boron network, demonstrating that the Li atom-modified borophene nanostructure materials could be used as a promising

Table 5 Hydrogen storage applications of borophene

Species	Coated metal	Binding energy (E_b) (eV)/ adsorption energy (E_{ads}) (eV)	Hydrogen storage capacity (%)	Ref.
Li-decorated β12 borophene	Li	−0.0704	2.70	127
$2Ca_4B_{20}(H_2)_{18}$	Ca	−1.52	9.5	128
$2Ca_4B_{16}(H_2)_{12}$	Ca	−1.06	7.2	
Borophene	Na	−0.34	9.0	129
	Li	−0.36	6.8	
	Ca	−0.12	7.6	
$B_{16}Ti_4$	Ti	0.199	15.065	130
N-doped borophene sheet	N	0.6	6.22	131
Borophene	Li	−1.15	13.96	132
	Na	−0.50		
	K	−1.19		
2Li-β12-borophene	Li	−0.220	10.85	133
Li decorated β12 borophene	Li	0.38	8.76	134
Li decorated χ3 borophene			10.79	
Li-doped borophene	Li	0.142	13.7	135
Borophene nanosheet	—	—	6.5	136
Mn atom/H-ZBNR	Mn	—	12	137
Co-atom/H-ZBNR	Co	—	8	
B_2O	Li	—	8.3	138

medium for hydrogen storage applications. The use of conductive borophene nanostructures as a material for the charge-controlled switchable H_2 storage has been suggested.[136] The author studied the adsorption ability of the charged borophene nanosheet for the capturing of the H_2 molecule using DFT calculations. In theory, a positive or negative charge of the borophene nanosheets have 6.5 wt% of H_2 storage capacity.[136]

Recently, magnetic features of unmodified zigzag borophene nanoribbon (ZBNR) and hydrogenated-ZBNR were investigated by non-equilibrium Green's function and DFT calculations.[137] These theories demonstrated that the non-magnetic nature of H-ZBNR was changed to magnetic H-ZBNR by the doping of the metal atoms, Mn and Co. Furthermore, the spin filtering efficiencies for the Mn atom/H-ZBNR and Co-atom/H-ZBNR were 12% and 8%, respectively. Similarly, the 2D honeycomb B_2O nanostructure was decorated with alkali metals (K, Na and Li) and their hydrogen storage capacity was studied.[138] The decoration of alkali metal atoms on the surface of the boron-containing nanostructure leads to the enhancement of the interaction with the hydrogen molecule. Among the metal atom-decorated B_2O, the Li-atom modified B_2O nanostructure exhibited higher theoretical gravimetric density (8.3 wt%) for hydrogen molecules, as compared with the Na- and K-atom modified B_2O nanostructure. These data illustrated that the Li-atom modified B_2O nanostructure could be used as an ideal material for hydrogen storage applications. Table 5 illustrates the applications of the borophene-based nanostructures for H_2 storage applications.

6. Summary and future perspectives

In this review, the history, synthetic approaches and properties of 2D borophene nanostructure materials have been summarized. In addition, we discussed the promising applications of 2D borophene nanostructures in sensing, Li- and Na-ion batteries and hydrogen storage devices. Various synthetic strategies successfully demonstrated the use of a synthetic route for the fabrication of 2D borophene nanostructures, which are well supported by the computational designs of borophenes. Furthermore, the findings from these research reports revealed that a large number of borophene allotropes exhibited outstanding properties (mechanical, structural, magnetic, electronic, optical, thermal conductivity), exploring them as one of the potential materials for various applications that can easily replace the use of graphene. Borophene differs from other 2D materials because the amount of boron vacancy defects is undefined, which causes an uncertain difference between the borophene crystals and boron vacancy defects. Importantly, the modification of the 2D borophene nanostructure with organic ligands and inorganic elements (N, alkali metals and transition metals) offers several features, such as specific interaction towards gas molecules, enhancement of optical properties and conductivity, generation of metallic nature and improvement of the adsorption of H_2 molecules, favoring various new applications (sensing, battery and H_2 storage devices). Moreover, the modification of borophene nanostructures with metal atoms has significantly improved the adsorption of H_2 molecules and allowed for the change from a nonmagnetic to magnetic nature. All of these features of the borophene nanostructure have proven to be a benchmark for the establishment of the 2D borophene chemistry with novel and remarkable applications in energy, catalysis, analytical and biomedical sciences, which could be either a novel sister of the 2D graphene or alternative to the 2D nanostructure materials (graphene and MXenes).

Although significant progress has been made in the theoretical chemistry of borophene, several elusive challenges should be resolved in borophene chemistry. In the literature, numerous computational and numerical approaches have successfully demonstrated the generation of 2D borophene. However, significant experimental studies must be focused on the preparation of 2D borophene nanostructures *via* simplified synthetic protocols, thereby producing 2D borophene with good stability and outstanding properties, which allows them to be used in practical applications. Very limited studies have been focused on the modification of borophene with a wide variety of ligands and nanocomposites. Thus, significant efforts must be devoted to the modification of borophene nanostructures with various types of ligands/metal atoms and nanocomposites, which greatly enhances their opportunities in multidisciplinary research areas. In addition, the applications of 2D borophene nanostructures should be expanded to all fields of science and technology. Similarly, the sensing applications of borophenes may be extended to other target molecules, such as organic, biomolecules and inorganic species, which enhance their utility in analytical sciences. Even though the synthesis and applications of borophene and its nanostructures are still in its infancy, new synthetic approaches for borophenes with novel properties will extend their practical applications in modern science, favoring a new avenue for the commercial adoption of borophene for various industrial applications. Finally, borophene is recognized as a rising star in

materials chemistry. New investigations will help to extend the applications of borophene nanostructure materials in multi-disciplinary research (energy, catalysis, analytical chemistry, biomedical sciences, nanoelectronics and materials science) in the near future.

Conflicts of interest

There are no conflicts to declare.

Acknowledgements

D. J. J. thanks the Director, SVNIT, Surat for providing a doctoral fellowship and infrastructural facilities to this work. S. K. K. acknowledges the financial support from the Department of Science and Technology (DST), Government of India (EMR/2016/002621/IPC) and the Board of Research in Nuclear Science (BRNS), ((37(2)/14/07/2015/BRNS/10401) Government of India for this work.

References

1 K. S. Novoselov, A. K. Geim, S. V. Morozov, D. Jiang, M. I. Katsnelson, I. V. Grigorieva, S. V. Dubonos and A. A. Firsov, *Nature*, 2005, **438**, 197–200.
2 M. Ziaee Bideskan, K. Forooraghi and Z. Atlasbaf, *Sci. Rep.*, 2021, **11**, 1–13.
3 K. Watanabe, T. Taniguchi and H. Kanda, *Nat. Mater.*, 2004, **3**, 404–409.
4 Y. Li, V. Garnier, P. Steyer, C. Journet and B. Toury, *ACS Appl. Nano Mater.*, 2020, **3**, 1508–1515.
5 H. A. Huy, Q. D. Ho, T. Q. Tuan, O. K. Le and N. Le Hoai Phuong, *Sci. Rep.*, 2021, **11**, 14374.
6 Z. Gholami and F. Khoeini, *Sci. Rep.*, 2021, **11**, 1–14.
7 G. Liu, X. L. Lei, M. S. Wu, B. Xu and C. Y. Ouyang, *J. Phys.: Condens. Matter*, 2014, **26**, 355007.
8 A. Molle, C. Grazianetti, L. Tao, D. Taneja, M. H. Alam and D. Akinwande, *Chem. Soc. Rev.*, 2018, **47**, 6370–6387.
9 R. Garcia-Diaz, J. Guerrero-Sánchez, H. N. Fernández-Escamilla and N. Takeuchi, *Appl. Surf. Sci.*, 2019, **467**, 261–267.
10 J. Fang, P. Zhao and G. Chen, *J. Phys. Chem. C*, 2018, **122**, 18669–18681.
11 X.-R. Hu, J.-M. Zheng and Z.-Y. Ren, *Front. Phys.*, 2017, **132**, 1–8.
12 L. Kong, K. Wu and L. Chen, *Front. Phys.*, 2018, **133**, 1–11.
13 V. Wang and W. T. Geng, *J. Phys. Chem. C*, 2017, **121**, 10224–10232.
14 Z. A. Piazza, H. S. Hu, W. L. Li, Y. F. Zhao, J. Li and L. S. Wang, *Nat. Commun.*, 2014, **5**, 3113.
15 X. Tang, W. Sun, C. Lu, L. Kou and C. Chen, *Phys. Chem. Chem. Phys.*, 2019, **21**, 617–622.
16 X. Liu, Z. Zhang, L. Wang, B. I. Yakobson and M. C. Hersam, *Nat. Mater.*, 2018, **17**, 783–788.
17 Y. An, J. Jiao, Y. Hou, H. Wang, R. Wu, C. Liu, X. Chen, T. Wang and K. Wang, *J. Phys.: Condens. Matter*, 2018, **31**, 065301.
18 M. Gao, Q.-Z. Li, X.-W. Yan and J. Wang, *Phys. Rev. B.*, 2017, **95**, 024505.
19 B. Feng, J. Zhang, Q. Zhong, W. Li, S. Li, H. Li, P. Cheng, S. Meng, L. Chen and K. Wu, *Nat. Chem.*, 2016, **8**, 563–568.
20 W. Li, L. Kong, C. Chen, J. Gou, S. Sheng, W. Zhang, H. Li, L. Chen, P. Cheng and K. Wu, *Sci. Bull.*, 2018, **63**, 282–286.
21 V. Shukla, J. Warna, N. K. Jena, A. Grigoriev and R. Ahuja, *J. Phys. Chem. C*, 2017, **121**, 26869–26876.
22 J. Oh, K. Lee and Y. Park, *Sci. Rep.*, 2021, **11**, 14916.
23 C.-S. Liu, X. Wang, X.-J. Ye, X. Yan and Z. Zeng, *J. Chem. Phys.*, 2014, **141**, 194306.
24 A. J. Mannix, X.-F. Zhou, B. Kiraly, J. D. Wood, D. Alducin, B. D. Myers, X. Liu, B. L. Fisher, U. Santiago, J. R. Guest, M. J. Yacaman, A. Ponce, A. R. Oganov, M. C. Hersam and N. P. Guisinger, *Science*, 2015, **350**, 1513–1516.
25 Q. Zhong, L. Kong, J. Gou, W. Li, S. Sheng, S. Yang, P. Cheng, H. Li, K. Wu and L. Chen, *Phys. Rev. Mater.*, 2017, **1**, 021001.
26 H. Li, L. Jing, W. Liu, J. Lin, R. Y. Tay, S. H. Tsang and E. H. T. Teo, *ACS Nano*, 2018, **12**, 1262–1272.
27 R. Wu, I. K. Drozdov, S. Eltinge, P. Zahl, S. Ismail-Beigi, I. Božović and A. Gozar, *Nat. Nanotechnol.*, 2018, **141**, 44–49.
28 M. Franchini, P. H. T. Philipsen and L. Visscher, *J. Comput. Chem.*, 2013, **34**, 1819–1827.
29 P. Császár and P. Pulay, *J. Mol. Struct.*, 1984, **114**, 31–34.
30 F. Jensen, *J. Chem. Phys.*, 2002, **116**, 7372–7379.
31 M. Güell, J. M. Luis, M. Solà and M. Swart, *J. Phys. Chem. A*, 2008, **112**, 6384–6391.
32 J. P. Perdew, K. Burke and M. Ernzerhof, *Phys. Rev. Lett.*, 1996, **77**, 3865.
33 G. T. te Velde, F. M. Bickelhaupt, E. J. Baerends, C. F. Guerra, S. J. van Gisbergen, J. G. Snijders and T. Ziegler, *J. Comput. Chem.*, 2001, **22**, 931–967.
34 L.-C. Xu, A. Du and L. Kou, *Phys. Chem. Chem. Phys.*, 2016, **18**, 27284–27289.
35 H. Shu, F. Li, P. Liang and X. Chen, *Nanoscale*, 2016, **8**, 16284–16291.
36 Q. Zhong, J. Zhang, P. Cheng, B. Feng, W. Li, S. Sheng, H. Li, S. Meng, L. Chen and K. Wu, *J. Phys.: Condens. Matter*, 2017, **29**, 095002.
37 G. P. Campbell, A. J. Mannix, J. D. Emery, T.-L. Lee, N. P. Guisinger, M. C. Hersam and M. J. Bedzyk, *Nano Lett.*, 2018, **18**, 2816–2821.
38 W. Li, L. Kong, C. Chen, J. Gou, S. Sheng, W. Zhang, H. Li, L. Chen, P. Cheng and K. Wu, *Sci. Bull.*, 2018, **63**, 282–286.
39 L. Zhu, B. Zhao, T. Zhang, G. Chen and S. A. Yang, *J. Phys. Chem. C*, 2019, **123**, 14858–14864.
40 H.-S. Tsai, C.-H. Hsiao, Y.-P. Lin, C.-W. Chen, H. Ouyang and J.-H. Liang, *Small*, 2016, **12**, 5251–5255.
41 B. Kiraly, X. Liu, L. Wang, Z. Zhang, A. J. Mannix, B. L. Fisher, B. I. Yakobson, M. C. Hersam and N. P. Guisinger, *ACS Nano*, 2019, **13**, 3816–3822.

42 A. Berisha, *Chem. Phys.*, 2021, **544**, 111124.
43 C. Hou, G. Tai, J. Hao, L. Sheng, B. Liu and Z. Wu, *Angew. Chem. Int. Ed.*, 2020, **132**, 10911–10917.
44 P. Ranjan, T. K. Sahu, R. Bhushan, S. S. Yamijala, D. J. Late, P. Kumar and A. Vinu, *Adv. Mater.*, 2019, **31**, 1900353.
45 H. Wang, D. An, M. Wang, L. Sun, Y. Li, H. Li, N. Li, S. Hu and Y.-B. He, *Mater. Adv.*, 2021, **2**, 3269–3273.
46 F. Zhang, L. She, C. Jia, X. He, Q. Li, J. Sun and Z. Lei, *RSC Adv.*, 2020, **10**, 27532–27537.
47 X. Ni, H. Huang, K.-H. Jin, Z. Wang and F. Liu, *J. Phys. Chem. C*, 2020, **124**, 6063–6069.
48 G. Tai, T. Hu, Y. Zhou, X. Wang, J. Kong, T. Zeng, Y. You and Q. Wang, *Angew. Chem., Int. Ed.*, 2015, **54**, 15473–15477.
49 J. Hao, G. Tai, J. Zhou, R. Wang, C. Hou and W. Guo, *ACS Appl. Mater. Interfaces*, 2020, **12**, 17669–17675.
50 Z. Zhang, Y. Yang, G. Gao and B. I. Yakobson, *Angew. Chem., Int. Ed.*, 2015, **54**, 13022–13026.
51 L. Wang, A. Kutana, X. Zou and B. I. Yakobson, *Nanoscale*, 2015, **7**, 9746–9751.
52 Q. Wei and X. Peng, *Appl. Phys. Lett.*, 2014, **104**, 251915.
53 J. Zhou and R. Huang, *J. Mech. Phys. Solids*, 2008, **56**, 1609–1623.
54 L. Shao, X. Duan, Y. Li, Q. Yuan, B. Gao, H. Ye and P. Ding, *Phys. Chem. Chem. Phys.*, 2019, **21**, 7630–7634.
55 Z.-Q. Wang, T.-Y. Lü, H.-Q. Wang, Y. P. Feng and J.-C. Zheng, *ACS Appl. Electron. Mater.*, 2019, **1**, 667–674.
56 J. Yuan, N. Yu, K. Xue and X. Miao, *RSC Adv.*, 2017, **7**, 8654–8660.
57 C. Zhong, W. Wu, J. He, G. Ding, Y. Liu, D. Li, S. A. Yang and G. Zhang, *Nanoscale*, 2019, **11**, 2468–2475.
58 X. Wang, R. Wu, T. Xu and Y. Gao, *Mater. Res. Express*, 2021, **8**, 065003.
59 B. Peng, H. Zhang, H. Shao, Z. Ning, Y. Xu, G. Ni, H. Lu, D. W. Zhang and H. Zhu, *Mater. Res. Lett.*, 2017, **5**, 399–407.
60 H. Zhong, K. Huang, G. Yu and S. Yuan, *Phys. Rev. B.*, 2018, **98**, 054104.
61 R. Peköz, M. Konuk, M. E. Kilic and E. Durgun, *ACS Omega*, 2018, **3**, 1815–1822.
62 Y. P. Zhou and J. W. Jiang, *Sci. Rep.*, 2017, **7**, 1–12.
63 H. Sun, Q. Li and X. G. Wan, *Phys. Chem. Chem. Phys.*, 2016, **18**, 14927–14932.
64 A. Kochaev, K. Katin, M. Maslov and R. Meftakhutdinov, *J. Phys. Chem. Lett.*, 2020, **11**, 5668–5673.
65 H. Xiao, W. Cao, T. Ouyang, S. Guo, C. He and J. Zhong, *Sci. Rep.*, 2017, **7**, 45986.
66 Z. Zhang, M. Zhou, T. Zhang, M. Yang, Q. Yang, J. Yu and Y. Zhang, *ACS Appl. Mater. Interfaces*, 2020, **12**, 19746–19754.
67 H. Wang, Q. Li, Y. Gao, F. Miao, X.-F. Zhou and X. G. Wan, *New J. Phys.*, 2016, **18**, 073016.
68 Z. Wang, T. Y. Lü, H. Q. Wang, Y. P. Feng and J. C. Zheng, *Phys. Chem. Chem. Phys.*, 2016, **18**, 31424–31430.
69 Y. Duo, Z. Xied, L. Wang, N. M. Abbasi, T. Yang, Z. Li, G. Hu and H. Zhang, *Coord. Chem. Rev.*, 2021, **427**, 213549.
70 A. Rubab, N. Baig, M. Sher and M. Sohail, *Chem. Eng. J.*, 2020, **401**, 126109.
71 K. Zhour, J. M. Otero-Mato, F. E. H. Hassan, H. Fahs, M. Vaezzadeh, E. López-Lago, L. J. Gallego and L. M. Varela, *J. Mol. Liq.*, 2020, **316**, 113803.
72 A. Rastgou, H. Soleymanabadi and A. Bodaghi, *Microelectron. Eng.*, 2017, **169**, 9–15.
73 M. Faghihnasiri, H. Jafari, A. Ramazani, M. Shabani, S. M. Estalaki and R. G. Larson, *J. Appl. Phys.*, 2019, **125**, 145107.
74 J. W. Jiang, X. C. Wang, Y. Song and W. B. Mi, *Appl. Surf. Sci.*, 2018, **440**, 42–46.
75 J. E. Padilha, R. H. Miwa and A. Fazzio, *Phys. Chem. Chem. Phys.*, 2016, **18**, 25491–25496.
76 B. Mortazavi, M. Makaremi, M. Shahrokhi, M. Raeisi, C. V. Singh, T. Rabczuk and L. F. C. Pereira, *Nanoscale*, 2018, **10**, 3759–3768.
77 C. Zhang, Z. Zhang, W. Yan and X. Qin, *Adv. Condens. Matter Phys.*, 2021, **2021**, 1–7, DOI: 10.1155/2021/3718040.
78 T. Abasi, A. Boochani and S. R. Masharian, *Int. Nano Lett.*, 2019, **10**, 33–41.
79 A. Mogulkoc, Y. Mogulkoc, D. Kecik and E. Durgun, *Phys. Chem. Chem. Phys.*, 2018, **20**, 21043–21050.
80 M. Ishaq, R. A. Shehzad, M. Yaseen, S. Iqbal, K. Ayub and J. Iqbal, *J. Mol. Model.*, 2021, **27**, 1–11.
81 M. Fazilaty, M. Pourahmadi, M. R. Shayesteh and S. Hashemian, *J. Phys. Chem. Solids*, 2021, **148**, 109683.
82 Y. Huang, S. N. Shirodkar and B. I. Yakobson, *J. Am. Chem. Soc.*, 2017, **139**, 17181–17185.
83 B. Feng, O. Sugino, R.-Y. Liu, J. Zhang, R. Yukawa, M. Kawamura, T. Iimori, H. Kim, Y. Hasegawa and H. Li, *Phys. Rev. Lett.*, 2017, **118**, 96401.
84 J. Y. Li, H. Y. Lv, W. J. Lu, D. F. Shao, R. C. Xiao and Y. P. Sun, *Phys. Lett. A*, 2016, **380**, 3928–3931.
85 V. Arefi, A. Horri and M. B. Tavakoli, *Comput. Theor. Chem.*, 2021, **1197**, 113159.
86 J. Shen, Z. Yang, Y. Wang, L. C. Xu, R. Liu and X. Liu, *Appl. Surf. Sci.*, 2020, **504**, 144412.
87 F. Opoku and P. P. Govender, *J. Phys. Chem. A*, 2020, **124**, 2288–2300.
88 J. Shen, Z. Yang, Y. Wang, L. C. Xu, R. Liu and X. Liu, *J. Phys. Chem. C*, 2021, **125**, 427–435.
89 Z. Yu, Y. Li, X. Yu and F. Chen, *ACS Appl. Nano Mater.*, 2020, **3**, 9961–9968.
90 J. Li, X. Chen, Z. Yang, X. Liu and X. Zhang, *J. Mater. Chem. C*, 2021, **9**, 1069–1076.
91 M. Fazilaty, M. Pourahmadi, M. Reza Shayesteh and S. Hashemian, *Chem. Phys. Lett.*, 2020, **741**, 137066.
92 C. S. Huang, A. Murat, V. Babar, E. Montes and U. Schwingenschlögl, *J. Phys. Chem. C*, 2018, **122**, 14665–14670.
93 S. Sabokdast, A. Horri, Y. T. Azar, M. Momeni and M. Bagher Tavakoli, *Phys. E*, 2020, **119**, 114026.
94 H. Cui, X. Zhang and D. Chen, *Appl. Phys. A: Mater. Sci. Process.*, 2018, **124**, 1–8.
95 L. T. Ta, I. Hamada, Y. Morikawa and V. A. Dinh, *RSC Adv.*, 2021, **11**, 18279–18287.

96 R. Bhuvaneswari and R. Chandiramouli, *Chem. Phys. Lett.*, 2018, **701**, 34–42.
97 V. Nagarajan and R. Chandiramouli, *J. Inorg. Organomet. Polym. Mater.*, 2018, **28**, 920–931.
98 A. Omidvar, *Comput. Theor. Chem.*, 2017, **1115**, 179–184.
99 C. Tasaltın, T. A. Türkmen, N. Tasaltın and S. Karakus, *J. Mater. Sci.: Mater. Electron.*, 2021, **32**, 10750–10760.
100 C. Hou, G. Tai, B. Liu, Z. Wu and Y. Yin, *Nano Res.*, 2021, **14**, 2337–2344.
101 C. Hou, G. Tai, Y. Liu, Z. Wu, Z. Wu and X. Liang, *J. Mater. Chem. A*, 2021, **9**, 13100–13108.
102 C. Hou, G. Tai, Y. Liu and X. Liu, *Nano Res.*, 2021, 1–8, DOI: 10.1007/s12274-021-3926-6.
103 J. C. Alvarez-Quiceno, R. H. Miwa, G. M. Dalpian and A. Fazzio, *2D Mater.*, 2017, **4**, 025025.
104 Y. Mu and S. D. Li, *J. Phys. Chem. C*, 2020, **124**, 28145–28151.
105 F. Zergani and Z. Tavangar, *J. Mol. Liq.*, 2020, **319**, 114343.
106 R. Wu, H. Xu, Y. Zhao, C. Zha, J. Deng, C. Zhang, G. Lu, T. Qin, W. Wang, Y. Yin, C. Zhu, L. Wang, G. Ouyang and W. Huang, *Energy Storage Mater.*, 2020, **32**, 216–224.
107 O. Folorunso, Y. Hamam, R. Sadiku, S. S. Ray and G. J. Adekoya, *Mater. Today Proc.*, 2021, **38**, 485–489.
108 Y. Wu, H. Li and J. Hou, *Comput. Mater. Sci.*, 2021, **190**, 110273.
109 I. Muhammad, U. Younis, H. Xie, A. A. Khan, A. Khaliq, A. Samad, U. Schwingenschlögl and Q. Sun, *Chem. Mater.*, 2021, **33**, 2976–2983.
110 S. Abdolhosseini, M. Boroun and M. Pourfath, *J. Phys. Chem. C*, 2021, **125**, 5436–5446.
111 Q. Li, J. Yang and L. Zhang, *J. Phys. Chem. C*, 2018, **122**, 18294–18303.
112 J. Yu, M. Zhou, M. Yang, Q. Yang, Z. Zhang and Y. Zhang, *ACS Appl. Energy Mater.*, 2020, **3**, 11699–11705.
113 M. Makaremi, B. Mortazavi and C. V. Singh, *Mater. Today Energy*, 2018, **8**, 22–28.
114 Y. Wu, B. Zhang and J. Hou, *Phys. Chem. Chem. Phys.*, 2021, **23**, 9270–9279.
115 M. I. Khan, A. Majid, N. Ashraf and I. Ullah, *Phys. Chem. Chem. Phys.*, 2020, **22**, 3304–3313.
116 P. Xiang, X. Chen, J. Liu, B. Xiao and L. Yang, *J. Phys. Chem. C*, 2018, **122**, 9302–9311.
117 B. Mortazavi, O. Rahaman, S. Ahzi and T. Rabczuk, *Appl. Mater. Today*, 2017, **8**, 60–67.
118 D. Rao, L. Zhang, Z. Meng, X. Zhang, Y. Wang, G. Qiao, X. Shen, H. Xia, J. Liu and R. Lu, *J. Mater. Chem. A*, 2017, **5**, 2328–2338.
119 H. R. Jiang, Z. Lu, M. C. Wu, F. Ciucci and T. S. Zhao, *Nano Energy*, 2016, **23**, 97–104.
120 X. Zhang, J. Hu, Y. Cheng, H. Y. Yang, Y. Yao and S. A. Yang, *Nanoscale*, 2016, **8**, 15340–15347.
121 J. Hu, C. Zhong, W. Wu, N. Liu, Y. Liu, S. A. Yang and C. Ouyang, *J. Phys.: Condens. Matter*, 2020, **32**, 065001.
122 S. Leng, X. Sun, Y. Yang and R. Zhang, *Mater. Res. Express*, 2019, **6**, 085504.
123 T. Huang, B. Tian, J. Guo, H. Shu, Y. Wang and J. Dai, *Mater. Sci. Semicond. Process.*, 2019, **89**, 250–255.
124 V. Shukla, R. B. Araujo, N. K. Jena and R. Ahuja, *Phys. Chem. Chem. Phys.*, 2018, **20**, 22008–22016.
125 P. Liang, Y. Cao, B. Tai, L. Zhang, H. Shu, F. Li, D. Chao and X. Du, *J. Alloys Compd.*, 2017, **704**, 152–159.
126 Y. Zhao, C. Ban, Q. Xu, S. H. Wei and A. C. Dillon, *Phys. Rev. B: Condens. Matter Mater. Phys.*, 2011, **83**, 035406.
127 I. Cabria, A. Lebon, M. B. Torres, L. J. Gallego and A. Vega, *Appl. Surf. Sci.*, 2021, **562**, 150019.
128 X. Chen, L. Wang, W. Zhang, J. Zhang and Y. Yuan, *Int. J. Hydrogen Energy*, 2017, **42**, 20036–20045.
129 S. Haldar, S. Mukherjee and C. V. Singh, *RSC Adv.*, 2018, **8**, 20748–20757.
130 T. Z. Wen, A. Z. Xie, J. L. Li and Y. H. Yang, *Int. J. Hydrogen Energy*, 2020, **45**, 29059–29069.
131 B. A. Baraiya, N. N. Som, V. Mankad, G. Wu, J. Wang and P. K. Jha, *Appl. Surf. Sci.*, 2020, **527**, 146852.
132 L. Wang, X. Chen, H. Du, Y. Yuan, H. Qu and M. Zou, *Appl. Surf. Sci.*, 2018, **427**, 1030–1037.
133 T. Liu, Y. Chen, H. Wang, M. Zhang, L. Yuan and C. Zhang, *Materials*, 2017, **10**, 894.
134 Y. Ji, H. Dong and Y. Li, *ChemistrySelect*, 2017, **2**, 10304–10309.
135 L. Li, H. Zhang and X. Cheng, *Comput. Mater. Sci.*, 2017, **137**, 119–124.
136 X. Li, X. Tan, Q. Xue and S. Smith, *Int. J. Hydrogen Energy*, 2019, **44**, 20150–20157.
137 A. Vatankhahan and T. Movlarooy, *Mater. Sci. Eng., B*, 2021, **273**, 115391.
138 P. Habibi, T. J. H. Vlugt, P. Dey and O. A. Moultos, *ACS Appl. Mater. Interfaces*, 2021, **13**, 43233–43240.